UNIVERSITAT POLITÈCNICA DE CATALUNYA
BARCELONATECH

# ADAPTIVE ENERGY MANAGEMENT FRONT-ENDS FOR VARIABLE-DISTANCE ASYMMETRIC WIRELESS POWER TRANSFER LINKS

**A Degree's Thesis**

**Submitted to the Faculty of the**

**Escola Tècnica d'Enginyeria de Telecomunicació de Barcelona**

**Universitat Politècnica de Catalunya**

**by**

**Núria Egidos Plaja**

**In partial fulfilment**

**of the requirements for the**

**DEGREE IN ELECTRONIC SYSTEMS ENGINEERING**

**Advisors: Eduard Alarcón and Elisenda Bou**

**Barcelona, July 2014**

# Abstract

Resonant Inductive Coupling Wireless Power Transfer (RIC-WPT) is a leading field of research due to the growing number of applications that can benefit from this technology: from biomedical implants to consumer electronics, fractionated spacecraft and electric vehicles amongst others. However, current applications are limited to symmetric point-to-point-links.

New applications of RIC-WPT emphasize the necessity to explore these links for different configurations: asymmetrical systems and multi-point RIC-WPT networks. Prediction of their behaviour and optimization of these links are required before their deployment; and correction of performance and adaptation to operation conditions are necessary to enhance power transfer once the link is operative. Besides, application of these new configurations requires a revision of existing models to ensure that analytical description matches actual behaviour of both antennas and the complete RIC-WPT link.

In this work, regarding aforementioned points, a critical comparison of antenna and link models is performed to guarantee model to actual behaviour correlation. Regarding verified models, response of a RIC-WPT link is characterized for different coupling scenarios to predict its behaviour. Then a design methodology to optimize an asymmetric RIC-WPT link is presented. Finally, an adaptive energy management system is proposed to enhance operation conditions once the link has been deployed.

# Resum

La transferència d'energia sense cables per acoblament ressonant inductiu (RIC-WPT) és un camp de recerca capdavanter degut al creixent nombre d'apliacions que es beneficien d'aquesta tecnologia: des d'implants biomèdics fins a l'electrònica de consum, tecnologia aeroespacial fraccionada i vehicles elèctrics entre d'altres. Tot i així, les aplicacions actuals es limiten a enllaços simètrics punt a punt.

Les noves aplicacions de RIC-WPT emfatitzen la necessitat d'explorar aquest tipus d'enllaços per a d'altres configuracions: sistemes asimètrics i xarxes RIC-WPT multipunt. És necessari predir el seu comportament i optimitzar-los abans de fer-ne el desplegament; un cop l'enllaç és operatiu, és necessari corregir-ne el rendiment i garantir-ne l'adaptació a les condicions de treball per tal de millorar la transferència de potència. A més d'això, l'aplicació d'aquestes noves configuracions requereix la revisió dels models existents per tal de garantir que la descripció analítica es correspon amb el comportament real, tant en el cas de l'antena com el de l'enllaç RIC-WPT al complet.

En aquest treball, tot seguint els punts anteriors, es presenta una comparació crítica dels models per a descriure l'antena i l'enllaç RIC-WPT per tal de garantir-ne la correlació amb el comportament real. Un cop verificada, es caracteritza la resposta de l'enllaç RIC-WPT per a diferents escenaris d'acoblament per a predir-ne el comportament. Després, es presenta una metodologia de disseny per a la optimització d'un enllaç RIC-WPT asimètric. Finalment, es proposa un sistema de gestió adaptativa d'energia amb l'objectiu de millorar les condicions d'operació en un enllaç ja implementat.

# Resumen

La transferencia de energía sin cables por acoplamiento resonante inductivo (RIC-WPT) es un campo de investigación líder debido al creciente número de aplicaciones que se benefician de esta tecnología: desde implantes biomédicos hasta la electrónica de consumo, tecnología aeroespacial fraccionada y vehículos eléctricos entre otras. Sin embargo, las aplicaciones actuales se limitan a enlaces simétricos punto a punto.

Las nuevas aplicaciones de RIC-WPT enfatizan la necesidad de explorar este tipo de enlaces para otras configuraciones: sistemas asimétricos y redes RIC-WPT multipunto. Es necesario predecir su comportamiento y optimizarlos antes de su desplegamiento; una vez el enlace está operativo, es necesario corregir su rendimiento y garantizar la adaptación a las condiciones de trabajo para mejorar la transferencia de potencia. Además, la aplicación de estas nuevas configuraciones requiere la revisión de los modelos existentes para garantizar que la descripción analítica se corresponde con el comportamiento real, tanto en el caso de la antena como el del enlace RIC-WPT al completo.

En este trabajo, según los puntos anteriores, se presenta una comparación crítica de los modelos que describen la antena y el enlace RIC-WPT para garantizar su correlación con el comportamiento real. Una vez esto se ha verificado, se caracteriza la respuesta del enlace RIC-WPT en distintos escenarios de acoplamiento para predecir su comportamiento. Después, se presenta una metodología de diseño orientada a optimizar un enlace RIC-WPT asimétrico. Finalmente, se propone un sistema de gestión adaptativo de energía con el objetivo de mejorar las condiciones de operación en un enace ya implementado.

## Acknowledgements

I would like to thank my project supervisors, Eduard Alarcón and Elisenda Bou, for giving me the chance to see what research consists of and putting myself to the test. I longed to start a project from scratch and end up with an acceptable comprehension of the subject and at least some answers to the many questions arisen.

Thanks to David Vidal and Mohammed Saad, Master student and PhD candidate respectively, for their help on simulation software and the time they devoted to share their experience. Thanks to professors Alberto Poveda, Francesc Guinjoan and Xavi Chavarria for their advice on power electronics; professor Rosa M. Fernández for her lectures on control theory and, moreover, for her enthusiasm; thanks to professor José M. Miguel for his guidance on analogue electronics and the way he urged us his students to seize the moment.

And finally, my special thanks to my family and friends for their encouragement, even during the final, whirlwind phase of the project.

# Revision history and approval record

DOCUMENT DISTRIBUTION LIST

| **Name** | **e-mail** |
|---|---|
| Núria Egidos | nuria.egidos@alu-etsetb.upc.es |
| Eduard Alarcón | eduard.alarcon@upc.edu |
| Elisenda Bou | elisenda.bou@upc.edu |

| Written by: | | Reviewed and approved by: | |
|---|---|---|---|
| Date | 07/2014 | Date | 07/2014 |
| Name | Núria Egidos | Name | Eduard Alarcón, Elisenda Bou |
| Position | Project Author | Position | Project Supervisor |

# Table of contents

# List of Figures

# List of Tables

# 1. Introduction

Energy constraints are a fundamental limitation of wireless and mobile devices [24], so a safe, effective and efficient power supply is required for these applications to be practicable. Wireless Power Transfer (WPT) technology can provide the required energy without the size, weight, safety and lifetime limitations related to batteries or cable charging [20].

WPT can be classified into radiative transfer, inductive coupling and resonant inductive coupling (RIC). The first can transfer only small power (in the order of milliwatts) because most of energy is wasted into free space; energy transfer can be increased with highly directional antennas, but that requires an uninterruptible line-of-sight and has harmful effects on health [18]. Regarding inductive coupling and RIC, both are harmless to humans (they involve non-radiative fields), require no direct line-of-sight and can achieve high power transfer efficiencies. While inductive coupling is limited to a very short range (several centimetres), RIC achieves promising power transfer efficiencies (above 80%) at the medium range (several meters) [10].

This project is focused on RIC-WPT technology. Its basic principle is that two separate, magnetically coupled resonators with a common resonant frequency (the same at which power transfer will occur) can exchange energy at a high power transfer efficiency. Resonators or coils are capacitive-loaded to achieve the desired resonant frequency [10].

Regarding technology evolution, WPT had a strong development in the late 20$^{th}$ century when mobile electronic devices (laptops, cell phones, PDAs) became popular. RIC-WPT is a more novel technology: advances to make it suitable for commercial applications arrived in 2007 [24]. Nowadays, it is a leading field of research due to the growing number of applications that can benefit from this technology: from biomedical implants to consumer electronics, fractionated spacecraft and electric vehicles amongst others [19]. However, current applications are limited to symmetric point-to-point-links.

New applications of RIC-WPT emphasize the necessity to explore these links for different configurations: asymmetrical systems and multi-point RIC-WPT networks. Prediction of their behaviour and optimization of these links are required before their deployment; and correction of performance and adaptation to operation conditions are necessary to enhance power transfer once the link is operative. Besides, application of these new configurations requires a revision of existing models to ensure that analytical description matches actual behaviour of both antennas and the complete RIC-WPT link.

In this work, a critical comparison of antenna and link models is performed to guarantee model to actual behaviour correlation (Chapter 2). Regarding verified models, response of a RIC-WPT link is characterized in terms of impedances and resonant frequencies for different coupling scenarios to predict its behaviour (Chapter 3). Then a design methodology to optimize an asymmetric RIC-WPT link is presented (Chapter 4).

Finally, an adaptive energy management system (consisting of an Automatic Impedance Matching network) is proposed to enhance operation conditions once the link has been deployed. In particular, the presented adaptive energy management system is focused on a Single-Input Multiple-Output (SIMO) link. Performance of this application will be is strongly dependant [7] on distance between nodes, (mis)alignment, operation frequency and interfering elements (either interfering objects or other nodes). Different coupling scenarios are considered to analyse and design the proposed system (Chapter 5).

A set of annexes is also included for a deeper understanding of the work performed:

- Appendix 0 is a compendium of variables used for simulation and their dimension. All figures in the project are obtained regarding values in this annex.
- Appendix 1 defines a design procedure to dimension loop antennas for the simulation models.
- Appendix 2 presents Simulink and PSPICE simulation models for AIM structure.
- Appendix 3 deals with dimension of open loop, AIM network.
- Appendix 4 shows a detailed design of control loop for adaptive energy management section.

# 2. A critical comparison of RIC-WPT models

Existing models for loop antenna and RIC-WPT links are currently applied to links in static conditions (with no change in coupling or load conditions). Configurations to be studied in this project (asymmetric, SIMO links) involve more challenging situations (for instance, a sudden change in distance or alignment between antennas); this requires a revision of existing models to ensure that analytical description matches actual behaviour of both antennas and the complete RIC-WPT link.

A critical comparison of models is performed as described in Figure 1.

Regarding loop antenna model, study in [3] is revisited and impedance expression is verified both with a finite element field solver (FEKO) and Matlab.

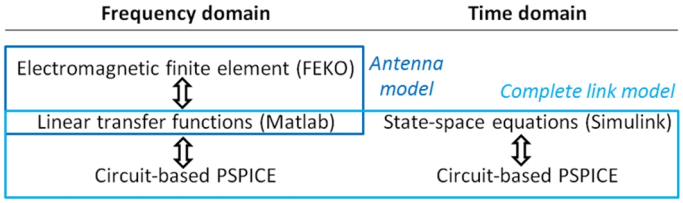


Figure 1 A critical comparison of models

Concerning RIC-WPT link analysis in [7], expressions in frequency domain are verified with the circuit-based PSPICE model and linear transfer functions in Matlab. Regarding time domain, a state-space equations model is presented and implemented with Simulink; its results are corroborated with the circuit-based, time domain PSPICE model.

## 2.1. Critical comparison of loop antenna impedance models

Two expressions for loop antenna impedance are presented in this section. The first is the complete version, including frequency-dependent capacitive and resistive losses, which has been used for frequency optimization chapter. The other version, which is used in the rest of the project, is a simplification of coil impedance for frequencies close to resonant frequency. Simplification consists of restricting resistive losses to a constant value, which is necessary for simulators with which it will be tested (Simulink, PSPICE).

### 2.1.1. Complete model of antenna impedance

Regarding [15], impedance of a loop antenna consists of the desired inductive component $L$ (which enables magnetic coupling), capacitive and resistive losses, as expressed in (1) and depicted at Figure 2:

$$Z_{coil}(\omega) = \frac{1}{j\omega C_{ext}} + \left( (j\omega L + R(\omega)) \,||\, \frac{1}{j\omega C} \right) \quad (1)$$

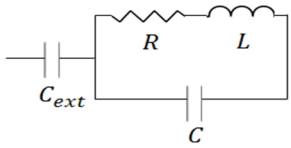


Figure 2 Impedance of a loop antenna

$C$ stands for the internal parasitic capacitance, while $C_{ext}$ is an external capacitor added to force coil resonance at the desired frequency.

Revisiting [3], resistive losses of an electrically small ($a \ll \lambda$) circular loop antenna (chosen for its low radiation resistance [30]) are considered. The losses of the resonator $R(\omega)$ depend upon its constituent materials ($\sigma, \delta$) and geometry ($a, b, c$) and can be divided into Radiative Losses ($R_r$), Ohmic Losses ($R_o$) and Dielectric Losses ($R_d$) [2]:

$$R = R_r + R_o + R_d \quad (2)$$

The radiation losses of a circular $N$-turn loop antenna with loop radius $a$ can be expressed as:

$$R_r = 20\pi^2 N^2 a^4 \frac{\omega^4}{{c_o}^4} \quad (3)$$

The ohmic resistance, which is in general much larger than the radiation resistance, depends upon the proximity effect (if the spacing between the turns in the loop antenna is small) and the skin effect. The total ohmic resistance for an $N$-turn circular loop antenna with loop radius $a$, wire radius $b$ and loop separation $2c$ is given by [2]:

$$R_o = \frac{N \cdot a}{b} R_s \cdot \sqrt{\frac{R_p}{R_0} + 1} \quad (4)$$

$R_s = \sqrt{\omega \mu_o / 2\sigma}$ is the surface impedance of the conductor and $R_p$ is the ohmic resistance per unit length due to proximity effect.

Finally, if a dielectric loop antenna is considered, the dielectric losses are given by:

$$R_d = \frac{tan\delta}{\omega C} = \omega L tan\delta \approx \omega 4\mu_o a N^2 tan\delta \quad (5)$$

$tan\delta$ is the loss tangent of the coil and $L$ has been approximated to $L = 4\mu_o a N^2$.

Losses can also be expressed as:

$$R_r = C_r \omega^4, C_r = \frac{20\pi^2 N^2 a^4}{{c_o}^4} \; ; R_o = C_o \sqrt{\omega}, C_o \approx \frac{Na}{b} \sqrt{\frac{\mu_o}{2\sigma}} \; ; R_d = C_d \omega, C_d \approx 4\mu_o a N^2 tan\delta \quad (6)$$

### 2.1.2. Coil impedance model restricted to resonant frequency

Resonator impedance expression can be simplified to an RLC series equivalent (Figure 3) in a narrow band around resonant frequency, $\omega \approx \omega_o$, for resonators with a high quality factor $Q = \omega_o \frac{L_s}{R_s} \approx \frac{R(\omega_o)}{\omega_o L}$ [26]. Expression for RLC series equivalent for $Q \gg 1$ and $\omega \approx \omega_o$ is the following:

$$Z_{coil}(\omega) \approx R_s + j\omega L_s + \frac{1}{j\omega C_s}$$
$$R_s \approx R(\omega_o)Q^2 \; ; L_s \approx L \; ; C_s \approx C||C_{ext} \qquad (7)$$

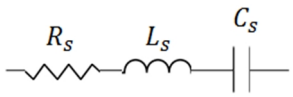


Figure 3 RLC series equivalent (narrow band) for impedance of a loop antenna

### 2.1.3. Verification of loop antenna impedance models

Figure 4 shows real and imaginary components of loop antenna impedance (normalized to their maximum) in respect of frequency normalized to resonant frequency of the coil; the simplified expression of losses in (6) for a dielectric-less coil ($R_d$ = 0) is represented. Superimposed results correspond to impedance measured with a finite element field solver (FEKO); impedance in (1) for $C_o$, $C_r$ parameters fitted with Matlab; and simplified version of coil impedance in (7).

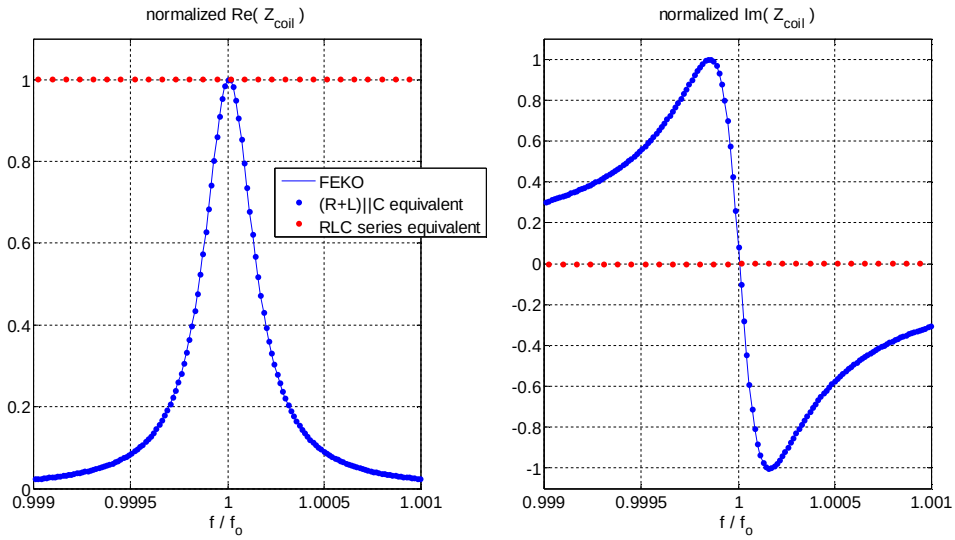


Figure 4 Coil impedance verification

It can be seen that analytical, complete model matches FEKO impedance, while the simplified model is valid only at resonant frequency.

Since analytical expression for antenna impedance has been verified in this section, it will be used in the coming chapters. Complete version of coil impedance is used for frequency optimization chapter, while simplified RLC series version is used for the rest of the project.

## 2.2. Critical comparison of RIC-WPT link models

Regarding the presented necessity to explore more generic, demanding link configurations, the RIC-WPT link considered in this project consists of loop antennas which can be asymmetric in size (diameter, number of turns), but not in technology [6], [7]. It is a SIMO link: a transmitter coil is coupled to multiple receivers; from the point of view of a particular one, the rest (or an interfering object which can be modelled as a loop antenna) will be considered as interfering coils. A general overview of this link is depicted at Figure 5 in terms of aforementioned narrow band equivalent of coil impedance (7) and the mutual inductances.

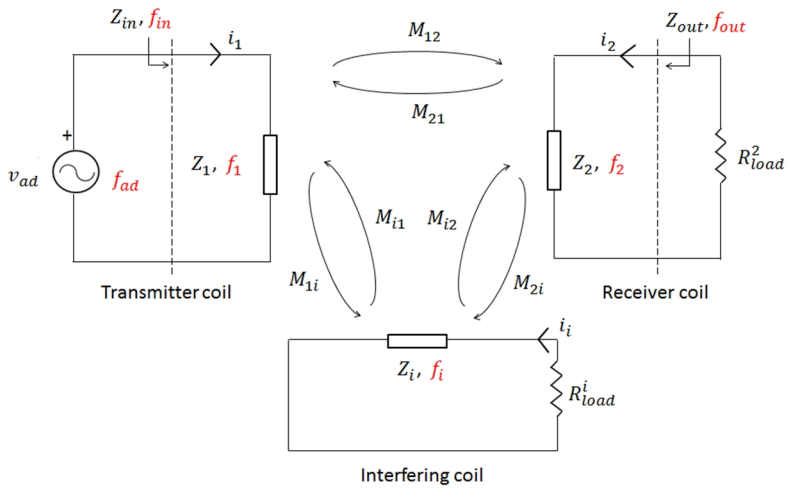


Figure 5 Generic RIC-WPT, SIMO link

$f_{1,2,i}$ stand for transmitter, receiver and interfering coil resonant frequencies respectively, and $f_{ad}$ is the operation frequency. Coupling effects between link components can be expressed in terms of phasor currents, mutually induced voltages and impedances [7].

This section introduces the critical comparison of models used to describe a RIC-WPT link (linear transfer functions, state-space equations, circuit-based PSPICE), whose results will be compared to verify correspondence between analytical model and actual response.

### 2.2.1. Linear transfer functions model

Frequency domain analysis of a RIC-WPT link in [7] relates phasor currents, mutually induced voltages and impedances in Figure 5 in order to describe the link behaviour. Equation system in (8) represents this interrelationship: $V_{ad}$ is the voltage source; $I_{1,2,i}$ stand for currents in transmitter, receiver and interfering coils respectively; $G_n$ are the coils transfer functions; and $G_{nm}$ is the transfer function for voltage induced in coil $m$ due current in coil $n$.

$$\begin{pmatrix} I_1 \\ I_2 \\ I_i \end{pmatrix} = \begin{pmatrix} 0 & G_1 \cdot G_{21} & G_1 \cdot G_{i1} \\ G_2 \cdot G_{12} & 0 & -G_2 \cdot G_{i2} \\ G_i \cdot G_{1i} & -G_i \cdot G_{2i} & 0 \end{pmatrix} \cdot \begin{pmatrix} I_1 \\ I_2 \\ I_i \end{pmatrix} + \begin{pmatrix} V_{ad} \cdot G_1 \\ 0 \\ 0 \end{pmatrix} \quad (8)$$

$$G_{nm} = \frac{V_{nm}}{I_n} \quad j \cdot \omega \cdot M_{nm} \; ; M_{nm} = k_{nm} \cdot \sqrt{L_n \cdot L_m}$$
$$G_n = \frac{I_n}{V_n} = \frac{1}{Z_n} \; ; Z_1 = R_1 + j \cdot \omega \cdot L_1 + \frac{1}{j \cdot \omega \cdot C_1} \; ; Z_{2,i} = R_{2,i} + R_{load}^{2,i} + j \cdot \omega \cdot L_{2,i} + \frac{1}{j \cdot \omega \cdot C_{2,i}} \quad (9)$$
$$n, m = 1,2, i$$

The former equation system can be translated to the block diagram in Figure 6 [7], from which analytical expressions to characterize the link in terms of input impedance and resonant frequencies are obtained.

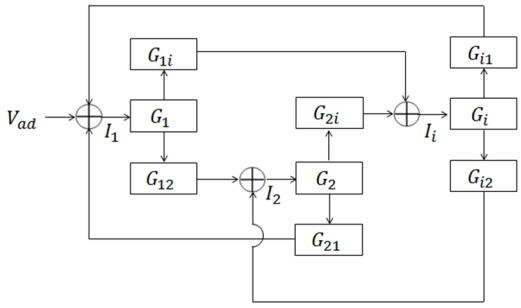


Figure 6 Block diagram model of a RIC-WPT link

### 2.2.2. State-space equations model

Time domain analysis of a RIC-WPT link can be performed in terms of state-space equations [4], which enable study of transient response, sudden changes in operation conditions and simulation of switching dynamics (which is required for adaptive energy management section).

State-space equations model considers capacitor, inductor and resistor voltages and coil currents defined in Figure 7. $v_{ad}$ stands for time domain voltage source and $v_{nm}$ is the induced voltage in coil $m$ due to current in coil $n$ (CCVS controlled by the current in the coil to which one is coupled).

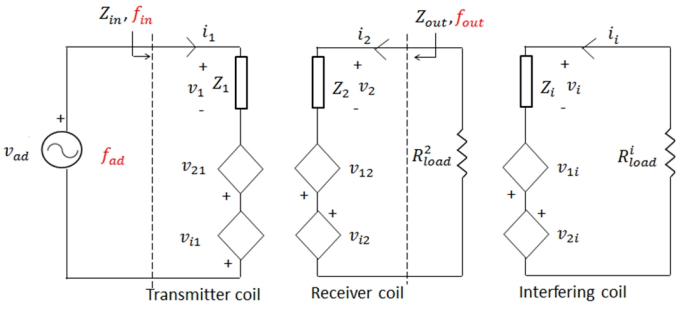


Figure 7 State-space equation model of a RIC-WPT link

This model is implemented with Simulink [1] as presented in Appendix 2 and its corresponding equations are the following:

$$v_{L_1} = v_{ad} + v_{21} + v_{i1} - v_{C_1} - v_{R_1}$$
$$v_{L_2} = v_{12} - v_{i2} - v_{C_2} - v_{R_2} - v_{R_{load}^2} \quad (10)$$
$$v_{L_i} = v_{1i} - v_{2i} - v_{C_i} - v_{R_i} - v_{R_{load}^i}$$

$$i_n = \frac{1}{L_n} \cdot \int v_{L_n}(t)dt \; ; v_{R_n} = i_n \cdot R_n \; ; v_{C_n} = \frac{1}{C_n} \cdot \int i_n(t)dt$$
$$v_{nm} = M_{nm} \cdot \frac{di_n}{dt} = \frac{M_{nm}}{L_n} \cdot L_n \cdot \frac{di_n}{dt} = \frac{M_{nm}}{L_n} \cdot v_{L_n} \quad (11)$$
$$n, m = 1,2, i$$

### 2.2.3. Circuit-based PSPICE model

Block diagram model is aimed to analytical expression derivation and frequency domain verification, while state-space equation model is aimed to time domain tests. Both of them are validated with circuit-based PSPICE model.

Circuit diagram in Figure 8 is a direct representation of a RIC-WPT link, in which coupling coefficient is implemented by means of the "K_linear" component (ANALOG library).

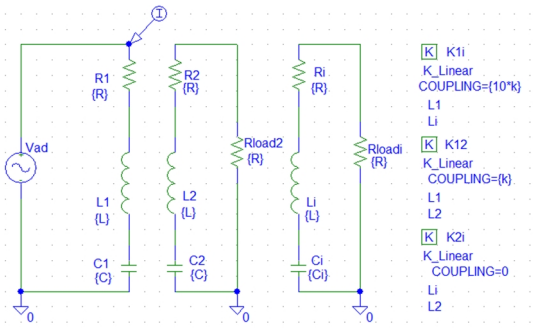


Figure 8 PSPICE model of RIC-WPT, SIMO link

### 2.2.4. Verification of RIC-WPT link models

This section presents verification results for RIC-WPT link models both in frequency and time domains. Figure 9 shows transmitted power in frequency domain for different coupling scenarios, comparing linear transfer function model implemented with Matlab and circuit-based PSPICE model; Figure 10 shows transmitter current comparing state-space equations model implemented with Simulink and circuit-based PSPICE model.

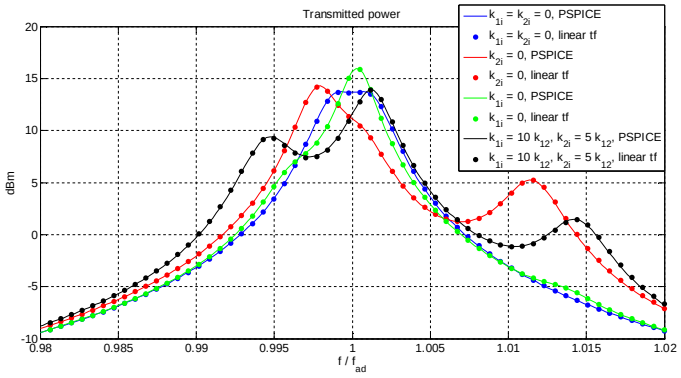


Figure 9 Frequency domain results for RIC-WPT link model verification

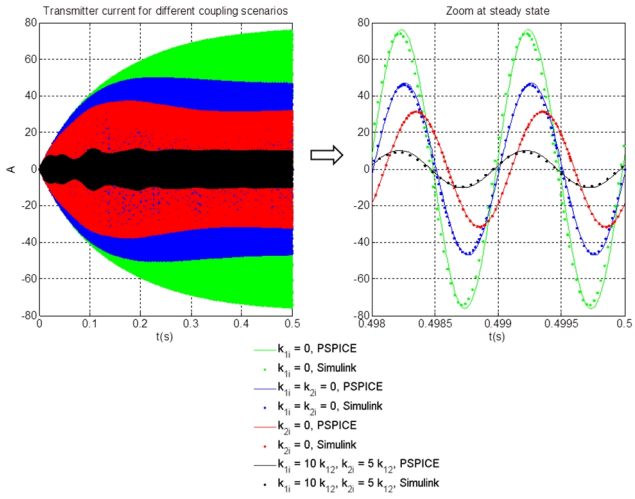


Figure 10 Time domain results for RIC-WPT link model verification

It can be seen that analytical models (linear transfer function, state-space equation) correspond to actual behaviour of a RIC-WPT link (circuit-based PSPICE). Therefore, prediction of link behaviour, design for an optimal performance and correction techniques to enhance performance for already deployed links can be based upon the existing models.

Since analytical models have been verified, results in the coming chapters will be presented only for linear transfer functions and state-space equations models.

# 3. Characterizing a RIC-WPT link

Once antenna and RIC-WPT link models have been verified, prediction of link behaviour for several coupling scenarios can be performed in terms of linear transfer function or block diagram model [7]. As it will be explained, link performance can be evaluated in terms of the link input impedance and its resonant frequency; transmitted power and transmitter to receiver coupling factor will also be considered for link characterization.

Link input impedance can be calculated solving (8):

$$Z_{in} = \frac{V_{ad}}{I_1} = \frac{1}{G_1} + \frac{G_2 \cdot G_{12} \cdot G_{21} + G_i \cdot G_{1i} \cdot G_{i1} - G_2 \cdot G_{2i} \cdot G_i \cdot G_{i1} G_{12} - G_2 \cdot G_{i2} \cdot G_i \cdot G_{1i} G_{21}}{G_2 \cdot G_i \cdot G_{2i} \cdot G_{i2} - 1} \quad (12)$$

If such a symmetry is assumed that $k_{nm} = k_{mn}$, $m, n = 1,2,i$, this expression is simplified to "reflected impedances" (from the coils to which one is coupled) for impedances defined in (9):

$$Z_{in} = \frac{V_{ad}}{I_1} = \frac{1}{G_1} + \frac{G_2 \cdot (G_{12})^2 + G_i \cdot (G_{1i})^2 - 2 \cdot G_2 \cdot G_{2i} \cdot G_i \cdot G_{1i} G_{12}}{G_2 \cdot G_i \cdot (G_{2i})^2 - 1} \quad (13)$$

$$\rightarrow Z_{in} = Z_1 + \frac{(\omega \cdot M_{12})^2}{Z_2 + \frac{(\omega \cdot M_{2i})^2}{Z_i}} + \frac{(\omega \cdot M_{1i})^2}{Z_i + \frac{(\omega \cdot M_{2i})^2}{Z_2}} - j \cdot \frac{2 \cdot \omega^3 \cdot M_{12} \cdot M_{1i} \cdot M_{2i}}{Z_2 \cdot Z_i + (\omega \cdot M_{2i})^2}$$

If all coupling factors are expressed in terms of transmitter to receiver coupling factor ($k_{nm}|_{nm \neq 12}^{n,m=1,2,i} \propto k_{12}$), then a critical coupling factor which maximizes power transfer at operation frequency can be defined. Furthermore, it is observed that critical coupling factor is also the frontier for link input impedance resonance split: for $k_{12} > k_{12}^c$, more than one resonance occurs in $Z_{in}$.

## 3.1. Critical coupling and power transfer

For a particular dimension of a RIC-WPT link, power transfer will depend upon coupling factor between transmitter and receiver ($k_{12}$) and the presence of an interfering coil. In order to evaluate the effects of the first, analysis is performed under the following conditions:

1) Definition of a critical coupling factor $k_{12}^c$ is restricted to operation frequency $f_{ad}$ and to a particular coupling configuration: a link with no interfering element ($k_{1i} = k_{2i} = 0$).
2) Transmitter and receiver resonance is matched to $f_{ad}$.
3) Mutual inductances are symmetric and they only differ in coupling factor, that is, $k_{12} = k_{21}$ and $L_1 = L_2$.

Under these conditions, power in receiver load at operation frequency can be expressed in terms of source voltage (phasor magnitudes), $k_{12}$ and quality factors defined as follows:

$$P_{load} = Re\{V_{load} \cdot I_2^*\} = \frac{|I_2|^2}{R_{load}^2}; \; I_2 = -\frac{G_{12}}{{G_{12}}^2 - \frac{1}{G_1 G_2}} V_{ad}|_{\omega = \omega_{ad}} = \frac{k_{12} C_2 \omega_{ad}}{{k_{12}}^2 + \frac{1}{Q_1 Q_2}} \quad (14)$$

$$Q_1 = \frac{1}{\omega_{ad} C_2 R_1}; \; Q_2 = \frac{1}{\omega_{ad} C_2 (R_2 + R_{load}^2)} \quad (15)$$

Receiver current $I_2$ has been obtained solving equation system in (8) and particularizing for conditions specified above. Maximizing receiver current will lead to maximum power at receiver load; therefore, $I_2$ derivative is calculated with respect to $k_{12}$ so as to obtain critical value of $k_{12}$:

$$\frac{d\, I_2(\omega_{ad})}{d\, k_{12}} = 0 \rightarrow\ k_{12}^c = \frac{1}{\sqrt{Q_1 Q_2}} \tag{16}$$

It can be seen that power in reception under these conditions is maximized for this value of transmitter to receiver coupling (Figure 11). A shift in $k_{12}$ from its critical value can be caused by a change in distance or alignment between transmitter and receiver [34], thus leading to a deterioration in link performance. Situations with $k_{12} < k_{12}^c$ are defined as undercoupling, while situations with $k_{12} > k_{12}^c$ are defined as overcoupling regime.

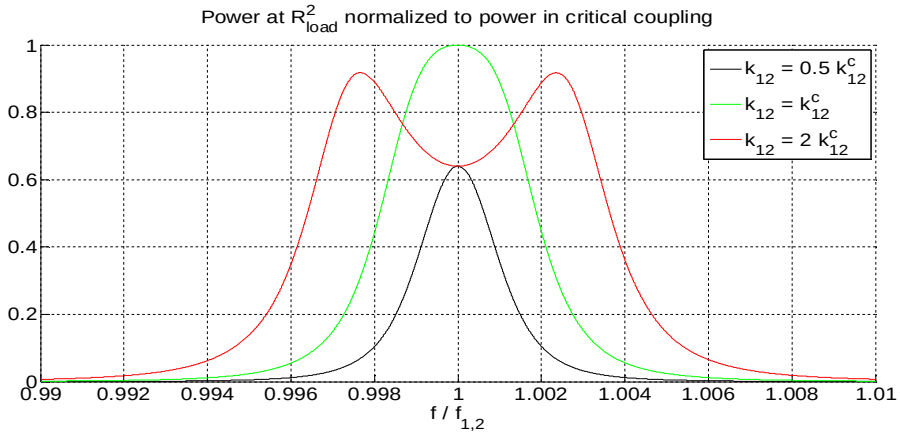


Figure 11 Evolution of load power as a function of frequency normalized to resonant frequency for different $k_{12}$ when $k_{1i} = k_{2i} = 0$

It is observed as well that $k_{12}^c$ is the frontier for a split in link input impedance resonant frequency, that is, the frequency in which imaginary component of $Z_{in}$ has a zero crossing (Figure 12 for situation $k_{1i} = k_{2i} = 0$ ). For aforementioned conditions, resonant frequency of $Z_{in}$ can be expressed in terms of (15) and critical coupling:

$$f_{in} = \frac{1}{2\pi\sqrt{L_1 C_1}} = f_{ad}\ \ \forall\, k_{12}$$

Additional resonances that appear if $k_{12} > k_{12}^c$ :

$$f_{in} = f_{ad}\sqrt{\frac{2 - \frac{1}{{Q_1}^2} \pm \sqrt{\frac{1}{{Q_1}^4} - \frac{4}{{Q_1}^2} + 4{k_{12}}^2}}{2\left(1-{k_{12}}^2\right)}} \xrightarrow{Q_1 \gg 1} f_{in} \approx f_{ad}\sqrt{1 \pm k_{12}}\ ,\ k_{12} > k_{12}^c \tag{17}$$

A frequency split in $f_{in}$is also observed for other link configurations as showed in Figure 12. This figure represents imaginary component of link input impedance, which has a zero crossing at its resonance (more than one zero crossing when there is resonance split). Situations with interfering coil coupled only to transmitter and with interfering coil coupled both to transmitter and receiver are superimposed in the central plot, for their result is very similar.

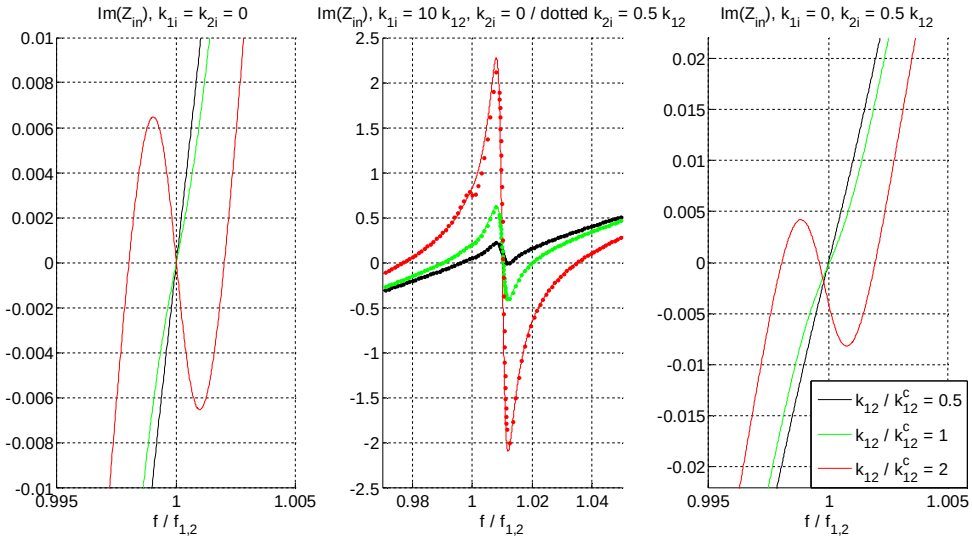


Figure 12 Evolution of $f_{in}$ (zero crossing of $Im(Z_{in})$) for different coupling scenarios

Not only a frequency split is observed in $f_{in}$ for situations different from the ideal configuration ($k_{12} = k_{12}^c$ , $k_{1i} = k_{2i} = 0$); as shown in Figure 12, "main resonance" (the closest to $f_{1,2}$) is shifted (if resonance of interfering coil is not matched to $f_{1,2}$).

Note that frequency shift in situations when interfering coil is coupled only to transmitter ($k_{2i} = 0$) or when it is coupled both to transmitter and receiver are very similar. This is due to the fact that mismatch caused by coupling to receiver is twice attenuated ($(\gamma_{2i}k_{12})^2$ times ${k_{12}}^2$), while that caused by coupling to transmitter is attenuated once ($(\gamma_{1i}k_{12})^2$); as a consequence, $k_{1i}$ effect prevails in both scenarios.

These results open a door to detect when a link is not operating at optimal conditions by analysing the link input impedance.

### 3.2. A way to measure performance deterioration in terms of link input impedance

In a RIC-WPT link operating at optimal conditions (transmitter and receiver are matched in frequency to operation frequency, $f_{1,2} = f_{ad}$; source and receiver loads are matched to link input and output impedances respectively), a deterioration in performance can be analysed in terms of link input impedance:

1) If there is a change in real component of $Z_{in}$
   Even though coils would still be tuned to operation frequency, a real component in $Z_{in}$ (purely resistive at operation frequency) different from nominal could lower power transfer. Regarding $Z_{in}$ expression, this can be caused by the following factors:
   1.1. A change in receiver load ($R_{load}^2$).
   1.2. Connection of multiple receivers to the transmitter, when all of them are matched in frequency to operation frequency (this introduces no imaginary component in $Z_{in}$).
   1.3. A change in distance or alignment between transmitter and receiver, which will change coupling factor $k_{12}$.

In this project, points 1.1. and 1.2. will not occur. Point 1.3. has already been analysed in the critical coupling factor section.

2) If there is a change in imaginary component of $Z_{in}$
   This will shift link input impedance resonant frequency away from $f_{ad}$ and even split it to multiple resonances. As a consequence, power transfer at operation frequency could be lowered. Regarding $Z_{in}$ expression, this can be caused by the following factors:
   2.1. Connection of an interfering coil which is not matched in frequency to operation frequency.

Connection of such an interfering coil as in 2.1. and its consequences (in terms of decrement in transmitted power) will be explained in detail.

Transmitted power can be expressed in terms of source voltage, transmitter current and angle of link input impedance (for phasor magnitudes) as follows:

$$P_{in} = Re\{V_{ad} \cdot I_1^*\} = |V_{ad}| \cdot |I_1| \cdot Re\{e^{j(\phi_{in})}\} = P_{in}|_{\phi_{in}=0} \cdot \cos(\phi_{in}) \quad (18)$$

$P_{in}|_{\phi_{in}=0}$ stands for the maximum power achievable in transmission for a particular coupling configuration. That is, transmitted power will be maximum if link input impedance has a 0º phase at operation frequency or, in other words, there is no phase mismatch between source voltage and transmitter current. On the other hand, the lowest transmitted power will occur for $\phi_{in} = \frac{\pi}{2}$.

This phase mismatch is a function of coupling coefficients and coil impedances. So as to simplify analysis, the following conditions are assumed:

1) Mutual inductances are symmetric and they only differ in coupling factor, that is, $k_{nm} = k_{mn}, n, m = 1,2, i$ and $L_1 = L_2 = L_i$.
2) Coupling scenarios to be considered are depicted at Figure 13. Ideal situation is a link with no interfering element ($k_{1i} = k_{2i} = 0$), since transmitted power is entirely captured by receiver. Situations when interfering coil is coupled to transmitter ($k_{2i} = 0$), to receiver ($k_{1i} = 0$) or both of them simultaneously will deteriorate performance, since interfering element will capture a portion of transmitted power.
3) Transmitter to receiver coupling factor is dimensioned as critical for nominal conditions ($k_{12} = k_{12}^c$), which will maximize power in receiver load. Besides, there will be no phase mismatch in situation $k_{1i} = k_{2i} = 0$ and phase mismatch in the rest of situations will be introduced by the interfering coil.

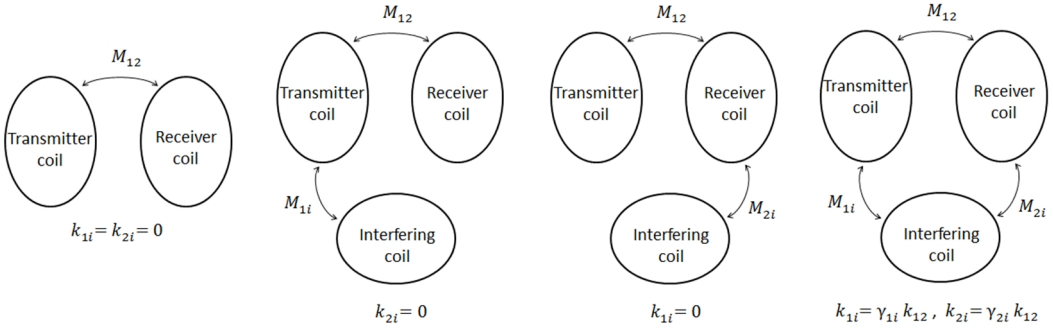


Figure 13 Definition of coupling scenarios

Regarding coupling scenarios with interfering element, phase mismatch introduced by an interfering coil at operation frequency (that is, phase of $Z_{in}$ at $f_{ad}$, which is denoted as $\phi_{in}$) can be expressed in terms of coupling factor $k_{12}$, divergence of interfering coil resonant frequency in respect of transmitter and receiver resonant frequency (Δ) and quality factors defined in (21). So as to provide a closed analytical expression for this mismatch, below are presented expressions for coupling scenarios when interfering coil is coupled only to transmitter or only to receiver:

$$\phi_{in}|_{k_{1i}=0} = \text{atan}\left(\frac{Im\{Z_{in}\}}{Re\{Z_{in}\}}\right)|_{k_{1i}=0}$$

$$\rightarrow \phi_{in}|_{k_{1i}=0}\ \text{atan}\left(-\frac{(\gamma_{2i}\cdot k_{12})^2\cdot\Delta\cdot(\Delta+2)}{\frac{1}{Q_2}\cdot\left(\frac{1}{Q_1Q_2}+{k_{12}}^2\right)\cdot\left(\frac{1}{{Q_i}^2}+(\Delta\cdot(\Delta+2))^2\right)+(\gamma_{2i}\cdot k_{12})^2\cdot\left(\frac{2}{Q_1Q_2Q_i}+{k_{12}}^2\cdot\left(\frac{{\gamma_{2i}}^2}{Q_1}+\frac{1}{Q_i}\right)\right)}\right) \quad (19)$$

$$\phi_{in}|_{k_{2i}=0} = \text{atan}\left(\frac{Im\{Z_{in}\}}{Re\{Z_{in}\}}\right)|_{k_{2i}=0} = \text{atan}\left(\frac{(\gamma_{1i}\cdot k_{12})^2\cdot\Delta\cdot(\Delta+2)}{Q_2\cdot\left(\frac{1}{Q_1Q_2}+{k_{12}}^2\right)\cdot\left(\frac{1}{{Q_i}^2}+(\Delta\cdot(\Delta+2))^2\right)+\frac{(\gamma_{1i}\cdot k_{12})^2}{Q_i}}\right) \quad (20)$$

$$\gamma_{1i,2i} = \frac{k_{1i,2i}}{k_{12}}\ ;\ \Delta = \frac{f_i - f_{1,2}}{f_{1,2}} \xrightarrow{L_i=L_{1,2}} \Delta = \sqrt{\frac{C_{1,2}}{C_i}} - 1$$

$$Q_1 = \frac{1}{2\cdot\pi\cdot f_{ad}\cdot R_1\cdot C_1}\ ;\ Q_2 = \frac{1}{2\cdot\pi\cdot f_{ad}\cdot(R_2+R_{load}^2)\cdot C_2}\ ;\ Q_i = \frac{1}{2\cdot\pi\cdot f_{ad}\cdot(R_i+R_{load}^i)\cdot C_2} \quad (21)$$

In order to evaluate the effect of coupling to an interfering coil, phase mismatch for analytical expressions above is swept in Figure 14 to Figure 17 for different relation of interfering load in respect of receiver load ($R_{load}^i/R_{load}^2$); coupling to interfering coil in respect of transmitter to receiver coupling ($\gamma_{1i} = k_{1i}/k_{12}$ and $\gamma_{2i} = k_{2i}/k_{12}$, with $k_{12} = k_{12}^c$); and mismatch of interfering resonant frequency in respect of transmitter and receiver resonant frequency ($\Delta = (f_i - f_{1,2})/f_{1,2}$).

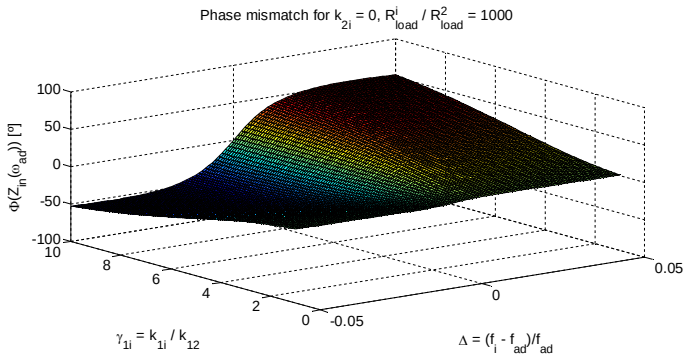


Figure 14 Phase mismatch for $k_{2i} = 0$, $R_{load}^i/R_{load}^2 = 10^3$

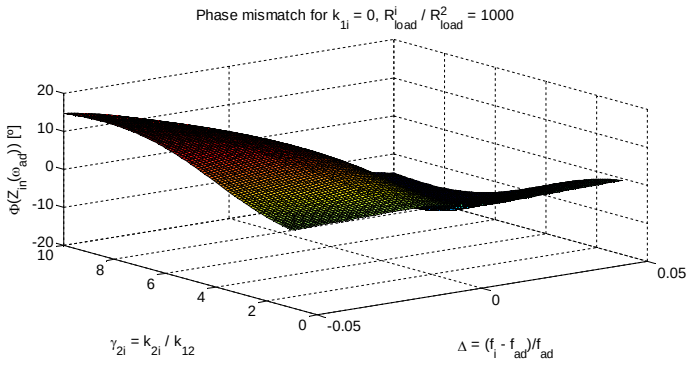


Figure 15 Phase mismatch for $k_{1i} = 0$, $R_{load}^i/R_{load}^2 = 10^3$

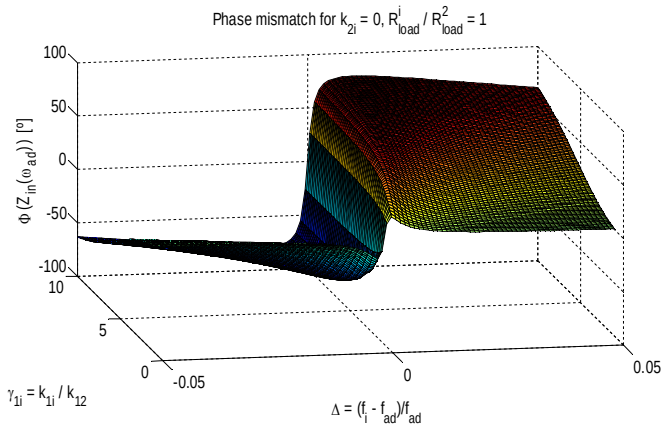


Figure 16 Phase mismatch for $k_{2i} = 0$, $R_{load}^{i}/R_{load}^{2} = 1$

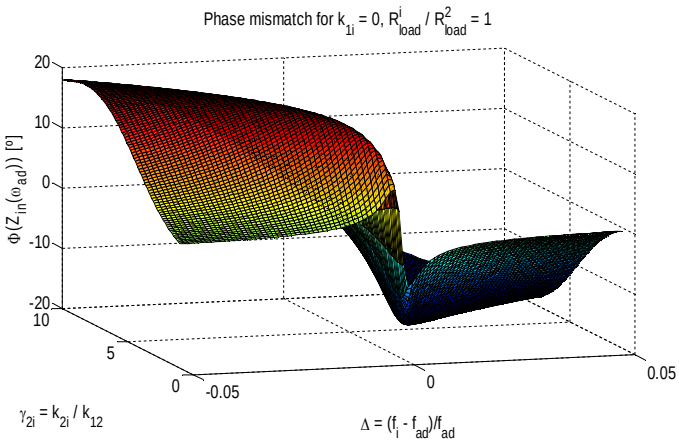


Figure 17 Phase mismatch for $k_{1i} = 0$, $R_{load}^{i}/R_{load}^{2} = 1$

It can be seen that phase mismatch is greater when interfering object is coupled to transmitter, since when it is coupled to receiver its effect is twice attenuated ($(\gamma_{2i}k_{12})^2$ times ${k_{12}}^2$). Involved resonators have a high quality factor, so phase mismatch is greater when interfering resonant frequency is very close to $f_{1,2}$ and for a small $R_{load}^{i}$ (for this increases $Q_i$ defined in (21)); in case of low quality factors, coils would not be strongly coupled and thus power transfer and effects derived from coupling (including phase mismatch) would be smaller.

# 4. Asymmetric link optimization

Power transfer efficiency is key in wireless power transfer systems. In particular, in RIC-WPT links, the efficiency of the physical layer strongly depends upon a) the frequency of operation (resonant frequency of the link), b) the losses of the transmitter and receiver coils and c) the mutual inductance between them. Since both the losses and the mutual inductance are frequency-dependant, it is of interest to analyse the optimal frequency at which a given link should operate to maximize its efficiency. This has been previously studied for symmetric point-to-point RIC-WPT links [3], [30], but it is still unexplored for asymmetrical configurations (different transmitter and receiver sizes), in which the difference between transmitter and receiver minimum-loss frequencies emphasize the need for an optimal system co-designed frequency of operation. In this chapter, the power transfer efficiency of impedance-matched asymmetric RIC-WPT links is studied in terms of frequency, and a closed analytical expression of the optimal frequency of operation is provided. Finally, the system efficiency of asymmetric frequency-optimized RIC-WPT links is analysed and compared to the symmetric frequency-optimized configuration.

## 4.1. Efficiency in asymmetric RIC-WPT

The power transfer efficiency in RIC-WPT links (composed of one transmitter and one receiver), defined as the ratio between the power delivered to the load and the total input power, can be expressed as a function of the input frequency $\omega$, the load $R_L$, transmitter and receiver losses ($R_1, R_2$), and the mutual inductance between them $M_{12}$ [21]:

$$\eta = \frac{R_L(\omega M_{12})^2}{(\omega M_{12})^2(R_2 + R_L) + R_1(R_2 + R_L)^2} \tag{22}$$

If impedance matching conditions are fulfilled ($R_L = \sqrt{{R_2}^2 + (\omega M_{12})^2 R_2/R_1}$, [8]), the efficiency of the system only depends upon the equivalent resistance of the coils (radiative, ohmic and dielectric losses), the mutual impedance between them and the frequency of operation, resulting in:

$$\eta_o = \frac{\sqrt{1+\left(\frac{\omega M_{12}}{\sqrt{R_1 R_2}}\right)^2}-1}{\sqrt{1+\left(\frac{\omega M_{12}}{\sqrt{R_1 R_2}}\right)^2}+1} = \frac{\sqrt{1+{S_a}^2}-1}{\sqrt{1+{S_a}^2}+1} \tag{23}$$

$$S_a = \frac{\omega M_{12}}{\sqrt{R_1 R_2}} \tag{24}$$

It can be observed in (23) that, to maximize efficiency, the relational factor $S_a$ -which is equivalent to the Coupled mode Theory $K/\Gamma$ [5] - has to be maximized.

To accomplish this, it is necessary to 1) maximize the frequency of the resonators ($\omega$), 2) maximize the mutual inductance between coils ($M_{12}$) and 3) minimize the transmitter ($R_1$) and receiver ($R_2$) losses, which depend upon the technological parameters of the coils and the separation between them as follows:

$$M_{12} = f(N_1, a_1, N_2, a_2, D_{12}) \;;\; R_1 = f(\omega, N_1, a_1, b_1, c_1, \sigma_1) \;;\; R_2 = f(\omega, N_2, a_2, b_2, c_2, \sigma_2) \tag{25}$$

where two circular loop antennas with $N_{1,2}$ turns, coil diameters $a_{1,2}$, wire radius $b_{1,2}$, inter-turn separation $c_{1,2}$, conductivity $\sigma_{1,2}$ and a distance $D_{12}$ between them have been assumed.

To maximize the efficiency, the frequency should be chosen so that $S_a$ is maximized (highest frequency, maximum mutual inductance and minimum coil losses). In the coming sections, the mutual inductance as well as the coil losses are derived for $N$-turn circular loop antennas.

### 4.1.1. Mutual Inductance

In the quasi-static limit, at large distances ($D_{12} \gg a_1$) the magnetic flux density at the receiver coil as a result of the transmitter coil has the form of a dipole [2]:

$$B_{12} \approx \frac{\mu_o}{2}\frac{N_1 i\, {a_1}^2}{{D_{12}}^3} \tag{26}$$

where coaxial orientation between coils has been assumed. The mutual inductance is then found from the flux through the $N_2$ linkages in the receiver coil:

$$M_{12} = N_2\frac{\partial \Psi_{12}}{\partial i} \approx \frac{\pi}{2} N_1 N_2 \mu_o \frac{{a_1}^2 {a_2}^2}{{D_{12}}^3} \tag{27}$$

### 4.1.2. Evaluation of Losses

Losses of the resonators depend upon their constituent materials ($\sigma_{1,2}$, $\delta_{1,2}$) and geometry ($a_{1,2}$ , $b_{1,2}$ , $c_{1,2}$) and can be divided into Radiative Losses ($R_r$), Ohmic Losses ($R_o$) and Dielectric Losses ($R_d$). As it has been presented in chapter 2.1 (Critical comparison of loop antenna impedance models), transmitter losses can be expressed as:

$$R_1 = R_r^1 + R_o^1 + R_d^1 \tag{28}$$

Defining the ratio of asymmetry in number of turns ($u_N$), antenna diameter ($u_a$), wire radius ($u_b$), inter-turn distance ($u_c$), conductivity ($u_\sigma$) and loss tangent ($u_\delta$) as follows:

$$u_N = \frac{N_2}{N_1};\ u_a = \frac{a_2}{a_1};\ u_b = \frac{b_2}{b_1};\ u_c = \frac{c_2}{c_1};\ u_\sigma = \frac{\sigma_2}{\sigma_1};\ u_\delta = \frac{\delta_2}{\delta_1} \tag{29}$$

the losses at the receiver (assuming $u_\delta = u_c = 1$) can be expressed as:

$$R_2 = R_r^2 + R_o^2 + R_d^2 = {u_N}^2 {u_a}^4 R_r^1 + \frac{u_N u_a}{u_b\sqrt{u_\sigma}} R_o^1 + u_a {u_N}^2 R_d^1 \tag{30}$$

## 4.2. Frequency optimization of asymmetric RIC-WPT

To find the optimal frequency at which the asymmetric RIC-WPT link should operate, it is necessary to take the derivative of $S_a$ with respect to $\omega$. To do this, the losses in the transmitter coil are expressed as presented in chapter 2.1 (Critical comparison of loop antenna impedance models):

$$R_1 = C_r^1 \omega^4 + C_o^1 \sqrt{\omega} + C_d^1 \omega \tag{31}$$

where $C_r^1$ , $C_o^1$ and $C_d^1$ are the frequency-independent coefficients corresponding to the radiation, ohmic and dielectric losses respectively. Similarly, the losses at the receiver coil can be defined as:

$$\begin{aligned} R_r^2 &= C_r^2 \omega^4;\ C_r^2 = K_r C_r^1;\ K_r = {u_N}^2 {u_a}^4 \\ R_o^2 &= C_o^2 \sqrt{\omega};\ C_o^2 = K_o C_o^1;\ K_o = \frac{u_N u_a}{u_b\sqrt{u_\sigma}} \\ R_d^2 &= C_d^2 \omega;\ C_d^2 = K_d C_d^1;\ K_d = u_a {u_N}^2 \end{aligned} \tag{32}$$

where $K_r$ , $K_o$ and $K_d$ model the effect of the asymmetries between transmitter and receiver upon the receiver's losses.

Finally, the mutual inductance can be expressed as a function of the equivalent mutual inductance obtained in a symmetric link ($u_{N,a,b,c,\sigma,\delta} = 1$) as:

$$M_{12}^a = K_m M_{12};\ K_m = u_N {u_a}^2 \tag{33}$$

Once this is known, both the mutual inductance (33) and the transmitter and receiver losses (31), (32) can be substituted in equation (24), resulting in the following expression for $S_a$:

$$S_a = \frac{\omega K_m M_{12}}{\sqrt{(C_r^1\omega^4 + C_o^1\sqrt{\omega} + C_d^1\omega)(K_r C_r^1\omega^4 + K_o C_o^1\sqrt{\omega} + K_d C_d^1\omega)}} \quad (34)$$

### 4.2.1. Optimal Frequency

$S_a$ is derived with respect to $\omega$ to obtain the optimal frequency at which the asymmetric link should operate. The resulting $\omega_{opt}^a$ is the solution of:

$$6\omega^7 {C_r^1}^2 K_r + 6\omega^4 C_d^1 C_r^1 \left(\frac{K_d+K_r}{2}\right) + 5\omega^{\frac{7}{2}} C_o^1 C_r^1 \left(\frac{K_o+K_r}{2}\right) - \omega^{\frac{1}{2}} C_d^1 C_o^1 \left(\frac{K_o+K_d}{2}\right) - K_o {C_o^1}^2 = 0 \quad (35)$$

For illustration purposes and in order to achieve a closed analytical formulation, dielectric-less transmitter and receiver coils are assumed ($C_d^1 = C_d^2 = 0$), obtaining:

$$\omega_{opt}^a = K_\omega \omega_{opt} \; ; K_\omega = \left(\frac{K_o+K_r}{K_r}\left[\sqrt{\frac{25}{16} + \frac{6K_oK_r}{(K_o+K_r)^2}} - \frac{5}{4}\right]\right)^{\frac{2}{7}} \quad (36)$$

where $\omega_{\text{opt}}$ is the optimal frequency corresponding to a symmetric link ($u_{N,a,b,c,\sigma,\delta} = 1$):

$$\omega_{opt} = \left(\frac{C_o^1}{6C_r^1}\right)^{\frac{2}{7}} \quad (37)$$

### 4.2.2. Maximum Efficiency

Once the optimal frequency at which the link should operate is obtained, the maximum relational factor $S_a$ and the resulting maximum efficiency $\eta_{max}^a$ can be found by substituting $\omega$ by $\omega_{opt}$ in (24):

$$S_{max}^a = S_{max} \frac{7K_m\sqrt{K_\omega}}{\sqrt{K_r {K_\omega}^7 + 6{K_\omega}^{\frac{7}{2}}(K_o+K_r)+36}} \quad (38)$$

where $S_{max}$ is the maximum relational factor $S$ for a symmetric link:

$$S_{max} = \frac{6M_{12}}{7C_o^1}\left(\frac{C_o^1}{6C_r^1}\right)^{\frac{1}{7}} \quad (39)$$

and the maximum power transfer efficiency is then obtained by:

$$\eta_{max}^a = \frac{\sqrt{1+{S_{max}^a}^2}-1}{\sqrt{1+{S_{max}^a}^2}+1} \quad (40)$$

### 4.2.3. Results

The results obtained above regarding the optimal frequency of the asymmetric link, the maximum relational factor $S_{max}^a$ and the corresponding maximum efficiency $\eta_{max}^a$ are illustrated below. First, the normalized optimal frequency deviation due to the link asymmetry is shown in Figure 18; it can be expressed as:

$$\Delta\omega = \frac{\omega_{opt}^a - \omega_{opt}}{\omega_{opt}} = K_\omega - 1 \; ; K_\omega = f(K_o, K_r) \text{ as per equation (36)} \quad (41)$$

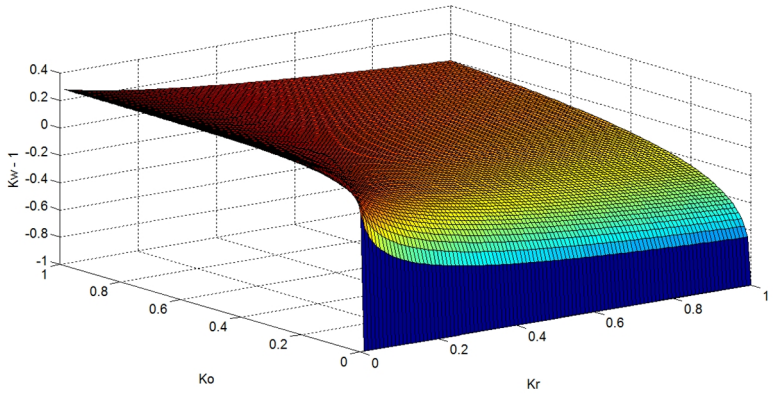


Figure 18 Normalized Frequency Deviation ($\Delta\omega$) with $C_o/C_r$ = 0.05

It can be observed that, when the asymmetry between transmitter and receiver represents around a 40% of difference either in the radiation or the ohmic losses, the optimal frequency of operation for the asymmetric link experiments a 20% deviation from the optimal frequency in the symmetric link, showcasing the impact of this study. When assessing the effect of the asymmetry in RIC-WPT links, it is also of interest to study how this asymmetry (described in a compressed manner by the coefficients $K_r$, $K_o$ and $K_m$) affects $S^a_{max}$ and the maximum achievable efficiency.

To do this, Figure 19 illustrates the obtained $S^a_{max}$ for different $K_o/K_r$ and $C_o/C_r$ coefficients as a function of frequency, where the frequency deviation explained in Figure 18 can be observed.

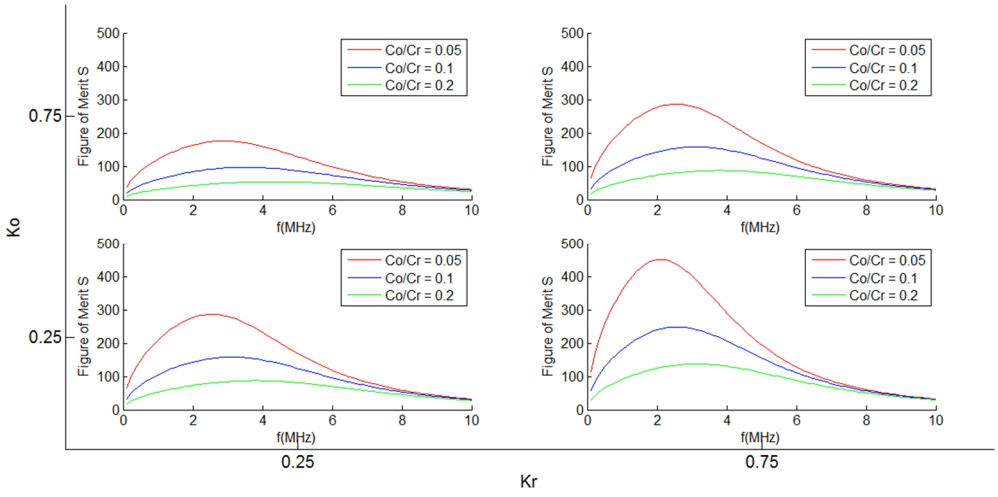


Figure 19 $S^a_{max}$ study for different $K_o$, $K_r$ configurations

Finally, Figure 20 shows the resulting maximum efficiency ($\eta^a_{max} = \eta^a|_{\omega=\omega^a_{opt}}$) normalized with respect to the symmetric link maximum efficiency ($\eta_{max} = \eta|_{\omega=\omega_{opt}}$). It can be observed that maximum efficiency is achieved for a symmetric link, and asymmetry in radiative losses causes the most significant deterioration in efficiency.

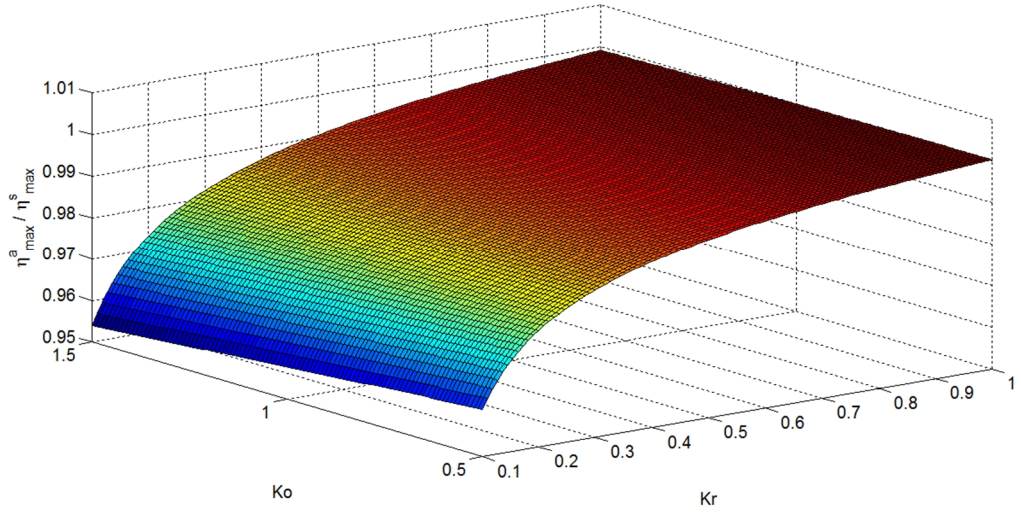


Figure 20 Normalized Maximum Efficiency for different $K_o$, $K_r$ configurations with $C_o / C_r$ = 0.05

# 5. Adaptive energy management in RIC-WPT

Due to the sensitivity of a RIC-WPT link to coil misalignment, change in distance, frequency mismatch or interfering objects [7], [32], a control structure is desired to stabilize the response in front of variation of link conditions. These are the required specifications for control structure:

- Provide stability in front of distance or alignment variation (which produces a change in coupling between the coils).
- Provide stability in front of an interfering object such that produces a shift in link resonant frequency.
- Provide impedance matching to the source and to the load to enable a matched link for maximum power transfer efficiency.
- Deliver the maximum power to the load (that is, not to dissipate the transferred power; this requires to implement a POPI network).
- Enable bidirectional power flow, which is a characteristic of WPT links.

Traditional approach to provide this functionality consists of RF impedance matching networks [29], for instance, $\pi$-matching networks. This requires component redesign when a change in operation conditions occurs (load variation, change in distance or alignment, etc.).

This chapter proposes an Automatic Impedance Matching network implemented via Power Factor Correction techniques, that is, an electronically tuneable system to accomplish aforementioned performance constraints and thus enhance power transfer.

## 5.1. Power Factor Correction techniques

As it has been presented in chapter 3.2. (A way to measure performance deterioration in terms of link input impedance), coupling an interfering element (whose resonant frequency is not matched to operation frequency) to transmitter or receiver coils will cause a non-zero phase of link input impedance at operation frequency, that is, a phase mismatch between voltage and current in transmitter side. PFC techniques are aimed to detect and correct that mismatch, and thus enhance performance in terms of power. To understand the operation principle of these techniques, their fundamentals and a survey on available configurations are presented.

Power Factor is defined as the ratio of real power (expressed in Watts) to apparent power (expressed in V·A) [27]: $PF = \frac{Real\ Power\ [W]}{Apparent\ Power\ [V \cdot A]}$.

Real power is the average (over a cycle) of the instantaneous product of voltage and current, and the apparent power is the product of the rms value of voltage times the rms value of current. In the present report conditions, both voltage and current are sinusoidal waveforms, and thus the power factor is the cosine of the phase difference. Therefore, Power Factor will be unitary when voltage and current are in phase.

The aim of Power Factor Correction techniques is to maximize Power Factor. The available techniques can be classified in two main groups [16], [33]:

- Passive techniques: consist of L-C filters, which is robust and does not produce EMI, but these are heavy and bulky configurations and cannot achieve very high Power Factor.
- Active techniques: these are composed of power electronics which match in phase the input current with the input voltage, achieving Power Factor close to unity (input interface emulates a pure resistor). They are lighter and smaller, but more complex.

Active techniques can be further classified into:

- PWM switching techniques: they are based on PWM converters, and their advantages are a simple configuration, analysis and control; and lowest voltage and current stress.
- Resonant converter techniques: their principle of operation is to shape the voltage across a switch or the current through a switch with an L-C structure to become zero before it is turned on or off, which reduces switching losses. They can operate at high switching frequencies. However, components are subject to higher stress.
- Soft-switching converter techniques: they combine PWM and resonant techniques by implementing an additional resonant network (L-C network and auxiliary switch). Their goal is to operate in PWM mode during the most of a switching period, and in resonant mode during the switch turn-on and turn-off intervals (therefore, the switch turns on and off at zero voltage or zero current conditions). This can reduce switching losses and component stress.

Regarding its well-known and extended use, and since it is suitable for this work purposes, PWM configuration is selected.

There are many control loop configurations available for PWM Power Factor Correction techniques [17], [31]. Below are listed some of the techniques to shape input current to input voltage that support CCM operation, which enables bidirectional current flow (a characteristic of WPT links):

- Hysteretic current mode control (for boost converter at CCM mode) [12]: it is a variable frequency architecture which controls inductor current switching.
- Peak current mode control (for boost converter at CCM mode and constant switching frequency): peak value of inductor current is sensed to regulate it in the next switching cycle. It requires slope compensation to stabilize the control system.
- Average current mode control (for boost converter at CCM mode and constant switching frequency) [25]: its basic principle is to shape the average value of inductor current to the average value of input voltage.

The most common configurations for PWM converters in these types of applications are buck, fly-back, Cuk and boost. Boost configuration is the most popular, since its input current (inductor current) can be easily sensed for current mode control purposes, and it is a continuous waveform at CCM mode (average current control is applicable and less EMI is produced); besides, the power switch is referenced to ground, which eases its control.

The selected configuration for the present work is a PWM PFC-based AIM network, composed of a boost converter and average current mode control loop.

## 5.2. AIM network overview

The structure of the proposed PFC-based AIM network to be implemented in transmitter front-end is depicted at Figure 21. It consists of a boost converter connected in series with transmitter antenna, and an average current mode control loop. Open-loop converter and control loop will be explained separately.

Principle of operation of this AIM network consists of shaping inductor current ($i_L = i_1$) to input voltage source ($v_{ad}$), that is, to achieve a 0º phase mismatch between voltage and current at the input of AIM structure or, in other words, a 0º phase in AIM network input impedance at operation frequency ($\phi_{in}^{AIM}(\omega_{ad}) = 0$). By doing this, voltage source will see an equivalent, resistive link input impedance, which will maximize power factor in transmitter front-end. This will increase transmitted power ($P_{in} = P_{in}|_{\phi_{in}=0}$ in (18)) and power at the load.

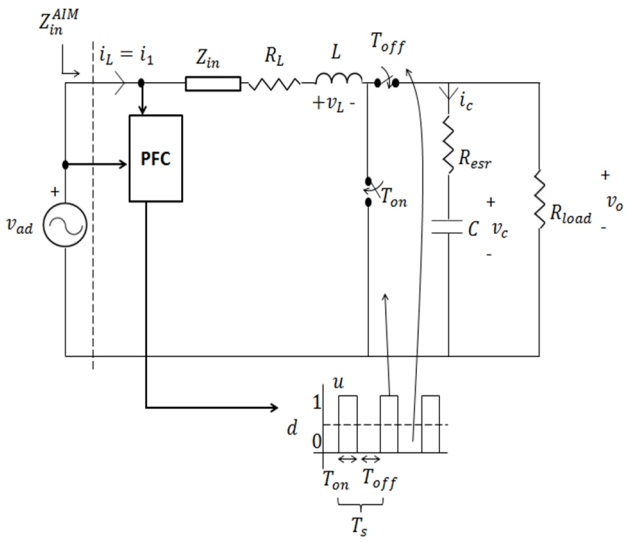


Figure 21 Structure of PFC-based AIM network implemented in transmitter front-end

### 5.2.1. Open-loop boost converter

Analysis and design of a CCM-operated boost converter have been widely studied [13]. Regarding the proposed configuration for AIM network, its input impedance is composed of the boost converter input impedance (averaged, CCM input impedance), in series with the link input impedance:

$$Z_{in}^{AIM}(s) = Z_{in}(s) + Z_{in}^{boost}(s) \tag{42}$$

$$Z_{in}^{boost}(s) = R_L + Ls + (1-D)^2 \left[ \left( R_{esr} + \frac{1}{Cs} \right) \;||\; R_{load} \right] \tag{43}$$

$R_L$ and $R_{esr}$ stand for inductor $L$ and capacitor $C$ losses respectively, and $R_{load}$ is the converter resistive load; $D$ is control signal (duty cycle) and $Z_{in}$ is link input impedance for the approximated model of coil impedance restricted to operation frequency (7).

The conventional theoretical approach in (43) will be valid as long as the output stage of boost converter behaves as a low pass filter, filtering switching frequency but preserving operation frequency. So as to achieve this, $f_s > 1/2\pi\sqrt{LC} > f_{ad}$.

In order to achieve the desired functionality, the following conditions must be accomplished:

1) Switches are bidirectional so as to enable CCM operation (and thus bidirectional current flow, a characteristic of WPT links).
2) It can be found a range of component and duty cycle values which provide a 0º phase in AIM input impedance at operation frequency:
   $Im\{Z_{in}^{boost}(\omega_{ad})\} = -Im\{Z_{in}(\omega_{ad})\} \rightarrow \phi_{in}^{AIM}(\omega_{ad}) = 0º$
3) It can be found a range of component and duty cycle values to provide a real component in $Z_{in}^{boost}(\omega_{ad})$ which is smaller than that of link input impedance:
   $Re\{Z_{in}^{boost}(\omega_{ad})\} \ll Re\{Z_{in}(\omega_{ad})\} \rightarrow P_{in} \approx P_{ad}$
   This will ensure that source power ($P_{ad}$) is injected mainly into the link ($P_{in}$).

An accurate description on dimension of boost components is provided in Appendix 3.

### 5.2.2. Control loop

PFC control loop is aimed to match in phase inductor current to voltage source (that is, to force 0º phase of $Z_{in}^{AIM}$ at $f_{ad}$); it is implemented with average current mode control configuration. Its operation principle is the following: averaged inductor current is compared to voltage to be tracked and then a control block is applied to error signal; this provides the proper control signal, the duty cycle which will drive boost converter switches. This leads to the desired boost input impedance, which will cancel link input impedance reactive component; as a result, equivalent input impedance of the link will be purely resistive.

Conventional average current mode control configuration includes a low pass filter which removes frequency components higher than operation frequency from inductor current to obtain its average value. However, this stage is not necessary for the proposed approach: since boost converter is connected in series to transmitter antenna (a high-Q band-pass filter), $i_L$ is already filtered to the desired frequency component. Besides, this intrinsic filtering will also remove ripple due to converter switching frequency.

Control loop structure is showed in Figure 22 and the corresponding expressions for block transfer functions are presented below. A more detailed explanation on control loop is provided in Appendix 4.

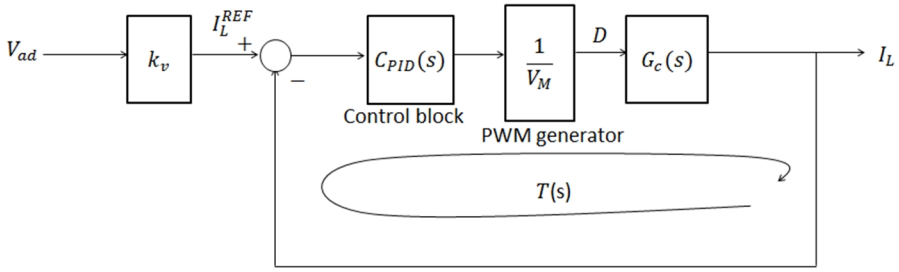


Figure 22 Block diagram of PFC control loop

Target signal of control loop is $v_{ad}$ scaled times $k_v$, a transconductance which adjusts it to the magnitude of filtered inductor current and thus enables a lower error. $C_{PID}$ is the control block described in (44), a PID controller with a high frequency pole ($\omega_p$) to make it practicable.

$$C_{PID}(s) = k_P + \frac{k_I}{s} + k_D \frac{\omega_p}{1+\frac{\omega_p}{s}} \tag{44}$$

$V_M$ stands for the peak-to-peak amplitude of the PWM comparator which generates the driving signal for converter switches. And duty cycle to inductor current transfer function ($G_c$) is obtained from small signal analysis of the proposed boost converter (solving for operation point $f_{ad}$, Appendix 4):

$$\begin{gathered} G_c(s) = \frac{i_L}{d} = \frac{V_{OP} + (1 - D_{OP}) I_{OP} Z_{par}}{Z_L + (1 - D_{OP})^2 Z_{par}} \\ Z_L = R_L + Ls\,; \quad Z_{par} = \left(R_{esr} + \frac{1}{Cs}\right) \| R_{load} \end{gathered} \tag{45}$$

$$V_{OP} = \frac{V_{in}^{boost}}{\frac{Z_L(\omega_{ad})}{(1-D_{OP})\,Z_{par}(\omega_{ad})} + (1-D_{OP})}\,;\; V_{in}^{boost} = V_{ad} - I_{OP} Z_{in}(\omega_{ad}) \tag{46}$$

$$I_{OP} = \frac{V_{OP}}{(1 - D_{OP})\, Z_{par}(\omega_{ad})} = \frac{V_{ad}}{Z_{in}(\omega_{ad}) + Z_L(\omega_{ad}) + (1 - D_{OP})^2 Z_{par}(\omega_{ad})} \tag{47}$$

$V_{OP}$, $I_{OP}$ and $D_{OP}$ stand for average output voltage of boost converter, average inductor current and duty cycle at operation frequency. Substituting $V_{OP}$ and $I_{OP}$ expression into (45) leads to:

$$G_c(\omega) = \frac{i_L}{d} = V_{ad} \frac{(1-D_{OP})\left[Z_{par}(\omega) + Z_{par}(\omega_{ad})\right]}{\left[Z_L(\omega) + (1-D_{OP})^2 Z_{par}(\omega)\right]\left[Z_{in}(\omega_{ad}) + Z_L(\omega_{ad}) + (1-D_{OP})^2 Z_{par}(\omega_{ad})\right]} \tag{48}$$

Finally, loop gain is obtained by multiplying aforementioned blocks transfer functions:

$$T(s) = C_{PID} \frac{1}{V_M} G_c \tag{49}$$

Then closed loop target voltage to inductor current transfer function can be expressed as:

$$H_c(s) = \frac{I_L}{V_{ad}} = k_v \frac{T}{1 + T} \tag{50}$$

Loop gain $T(s)$ is desired to be large so as to ensure a proper tracking of target signal.

Note that, in addition to PFC functionality, the proposed control loop also provides regulation in front of a change in coupling factor between link nodes. A case of interest (explained in section 3.1. Critical coupling and power transfer) is a variation in $k_{12}$ caused by a change in distance or alignment between transmitter and receiver, which would change critical $k_{12}$ and thus link would not operate at optimal conditions anymore. Since averaged $i_L = i_1$ is forced to be $k_v v_{ad}$ , transmitter current amplitude remains the same and operation at critical coupling is maintained.

## 5.3. Simulation

Former chapters have been devoted to prediction of a RIC-WPT link response for several coupling scenarios; design of an optimal dimension in nominal conditions; and design of an AIM network to enhance power transfer once the link has been deployed. This section presents simulation of the proposed AIM configuration so as to verify the performed analytical study. Operation conditions in front of which AIM network will provide robustness and enhance power transfer are presented and simulated, and results are benchmarked with those of a link with no AIM network, in order to verify performance improvement.

Simulation link is dimensioned to operate at optimal conditions: $k_{12} = k_{12}^c$ for maximum power transfer; and $R_{load}^2 = \sqrt{{R_2}^2 + (\omega M_{12})^2 \, R_2 / R_1}$ for impedance matching, [8], while interfering coil is dimensioned to produce a phase mismatch in link input impedance: $\gamma_{1i,2i} = k_{1i,2i}/k_{12}$ and $\Delta = (f_i - f_{1,2})/f_{1,2}$ are dimensioned regarding Figure 14 to Figure 17. Simulation link operation frequency is $f_{ad,1,2} = 1kHz$ (for illustration purposes).

Dimension of link components is presented in Appendix 0, while a complete description of simulation models is provided in Appendix 2.

### 5.3.1. Definition of simulation cases

Three main situations are considered to evaluate AIM network performance:

1) Several coupling scenarios (as described in Figure 13) for a static coupling factor, which will prove if AIM network can correct phase mismatch caused by an interfering coil.
2) Link with no interfering object, with a sudden change in distance or alignment between transmitter and receiver. This is emulated by means of a step in $k_{12}$; assuming transmitter and receiver come closer, $k_{12}$ changes to a higher value at half the simulation time. This case will prove if AIM network can maintain a constant transmitter current amplitude (and thus a constant transmitted power), which is desired to keep the link operating at optimal conditions (critical transmitter to receiver coupling factor).
3) Link with no interfering object, with switching frequency dimensioned too close to operation frequency. In this case, frequency separation between the different dynamics of the system, which is required for a boost-like behaviour of AIM network (section 5.2.1. Open-loop boost converter), is no longer accomplished. Obtained waveforms will not match the expected shapes and deterioration of performance will be evaluated.

### 5.3.2. Definition of magnitudes to be evaluated

The main goal of proposed AIM structure is to guarantee that voltage source connected to transmitter antenna will see a constant, resistive impedance regardless the coupling scenario, which will maximize power factor in transmitter front-end and thus power transfer. This section defines magnitudes to be measured in order to evaluate the benefits of implementing an AIM network, which are the following:

1) Link input impedance, comparing configuration without (13) and with AIM network (42).
2) Average and RMS power injected into the link (sinusoid magnitudes [13]). In case of no AIM network, they can be expressed in terms of transmitter current and the phase of link input impedance:

$$P_{in,average} = \frac{1}{2}|V_{ad}||I_1|\cos(\phi_{ad} - \phi_1) = \frac{1}{2}|I_1|^2|Z_{in}|\cos(\phi_{in})$$
$$P_{in,RMS} = \frac{1}{2}|V_{ad}||I_1| = \frac{1}{2}|I_1|^2|Z_{in}| \; ; I_1 = V_{ad}/Z_{in} \quad (51)$$

And for situation with AIM network, powers are expressed as follows:

$$P^{AIM}_{in,average} = \frac{1}{2}|I_1|^2\left|Z^{AIM}_{in}\right|\cos(\phi^{AIM}_{in}) \; ; P^{AIM}_{in,RMS} = \frac{1}{2}|I_1|^2\left|Z^{AIM}_{in}\right| \; ; I_1 = V_{ad}/Z^{AIM}_{in} \quad (52)$$

The increment in link input, average power which is achieved with AIM network will be measured as follows:

$$\Delta P_{in} = \frac{P^{AIM}_{in,average} - P_{in,average}}{P_{in,average}} \cdot 100 \quad (53)$$

3) Power Factor in transmitter front-end, which is defined as follows for situations without and with AIM network:

$$PF_{in} = \frac{P_{in,average}}{P_{in,RMS}} = |\cos(\phi_{in})| \; ; PF^{AIM}_{in} = \frac{P^{AIM}_{in,average}}{P^{AIM}_{in,RMS}} = \left|\cos\left(\phi^{AIM}_{in}\right)\right| \; ; 0 \leq PF_{in}, PF^{AIM}_{in} \leq 1 \quad (54)$$

4) Average power at the load (sinusoid magnitudes [13]), which is defined as follows:

$$P_{load,average} = \frac{1}{2}|I_2|^2 R_{load,2} \quad (55)$$

$I_2$ is defined in terms of $I_1$ by solving equation system in (8) (and then particularizing for the coupling scenarios to be simulated):

$$I_2 = \frac{G_{12} + G_i G_{i2} G_{1i}}{\frac{1}{G_2} - G_2 G_{i2} G_{2i}} I_1 \quad (56)$$

Analogously to link input power, the increment in load, average power which is achieved with AIM network will be measured as follows:

$$\Delta P_{load} = \frac{P^{AIM}_{load,average} - P_{load,average}}{P_{load,average}} \cdot 100 \quad (57)$$

### 5.3.3. Simulation results

This section presents simulation results in frequency and time domains for aforementioned simulation cases. Frequency domain results correspond to linear transfer functions model implemented with Matlab, while time domain results are obtained with state-space equations model implemented with Simulink.

#### 5.3.3.1. Results for situation 1: several coupling scenarios, static coupling factor

Results are evaluated in frequency and time domains (Figure 23 and Figure 24 respectively). Figure 23 shows phase of link input impedance with and without AIM network for the different coupling scenarios with a static coupling factor. It can be seen that phase mismatch at operation frequency caused by an interfering coil (whose resonant frequency is not matched to operation frequency) can be corrected with the proposed AIM network, thus achieving the desired performance enhancement.

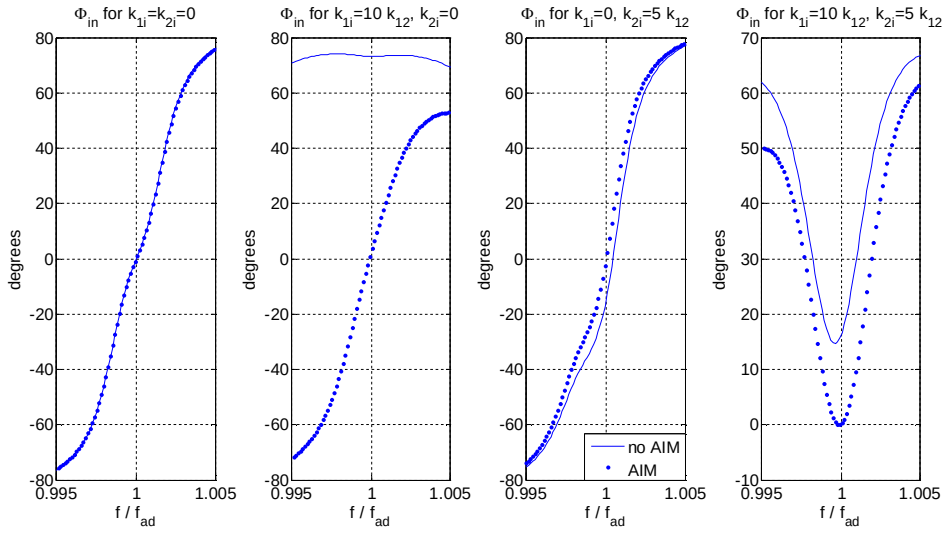


Figure 23 $\phi_{in}$ , $\phi_{in}^{AIM}$ obtained with coil impedance model restricted to operation frequency, simulation case 1

The same is observed in time domain: Figure 24 shows transmitter current waveform and voltage source for the different coupling scenarios, comparing a link with and without AIM network. On the left, full simulation results are shown. On the right top, a zoom in steady state for transmitter current for no AIM action (normalized to its maximum so as to compare it to voltage source); on the right bottom, a zoom in steady state for transmitter current with AIM action (not normalized).

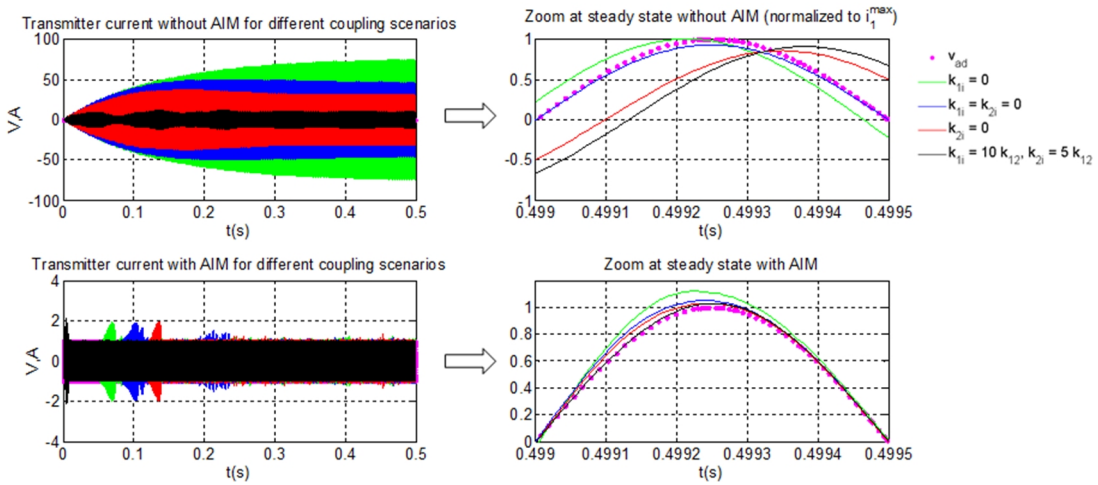


Figure 24 $v_{ad}$ , $i_1$ for simulation case 1: several coupling scenarios, static coupling factor

It can be seen that phase mismatch between voltage source and transmitter current caused by an interfering coil is corrected thanks to AIM action. Besides, results with AIM network confirm that transmitter current amplitude is fixed to $k_v v_{ad}$ whatever the coupling scenario, so optimal operation conditions are maintained. As it has already been commented, no ripple is observed in inductor current, for it is filtered by transmitter resonator.

Finally, Table 1 summarizes results in terms of phase mismatch correction, transmitted and load power increment and Power Factor improvement.

**Table 1 Results for simulation case 1**

| *Coupling scenario* | $\phi_{in}$ / $\phi_{in}^{AIM}$(º) | $\Delta P_{in}$(%) | $\Delta P_{load}$(%) | $PF_{in}$ / $PF_{in}^{AIM}$ |
|---|---|---|---|---|
| $k_{1i}$ = $k_{2i}$ = 0 | 0 / 0.03 | -0.99 | -1.86 | 1 / 0.99 |
| $k_{2i}$ = 0 | 73.12 / 0.81 | 96.83 | 86.71 | 0.29 / 0.99 |
| $k_{1i}$ = 0 | -14.69 / 0.03 | 4.5 | 4.06 | 0.96 / 0.99 |
| $k_{1i}$ = 10$k_{12}$, $k_{2i}$ = 5$k_{12}$ | 16.7 / 0.31 | 7.86 | 6.75 | 0.96 / 0.99 |

Verifying expected results, AIM network increments Power Factor in transmission, and thus transmitted power and power at the load, when there is an interfering coil in the link. Transmitted power and power at the load are slightly lowered in configuration implementing AIM network when there is no interfering coil, that is, nominal operation conditions; this is due to the fact that power injected into the link is shared between antenna and AIM network.

Promising power transfer increments are obtained with AIM network when interfering coil is coupled only to transmitter. A substantial, but more moderate improvement is obtained when interfering coil is coupled only to receiver or both to transmitter and receiver; this is explained because in these coupling situations receiver front-end is detuned as well, but adaptive energy management action is implemented only in transmission.

### 5.3.3.2. Results for situation 2: sudden change in distance/alignment

A change in $k_{12}$ (a step from $k_{12}^c$ to five times this value at half the simulation time) caused by a change in distance or alignment between transmitter and receiver is simulated. When the change occurs, amplitude of open loop $i_1$ is drastically reduced, for the link is now operating in over-coupling regime, and this leads to a decrement in power transfer. Figure 25 shows results from state-space equations model (implemented with Simulink) for a link with no interfering object in which the former change occurs; waveforms for configuration without and with AIM network are compared.

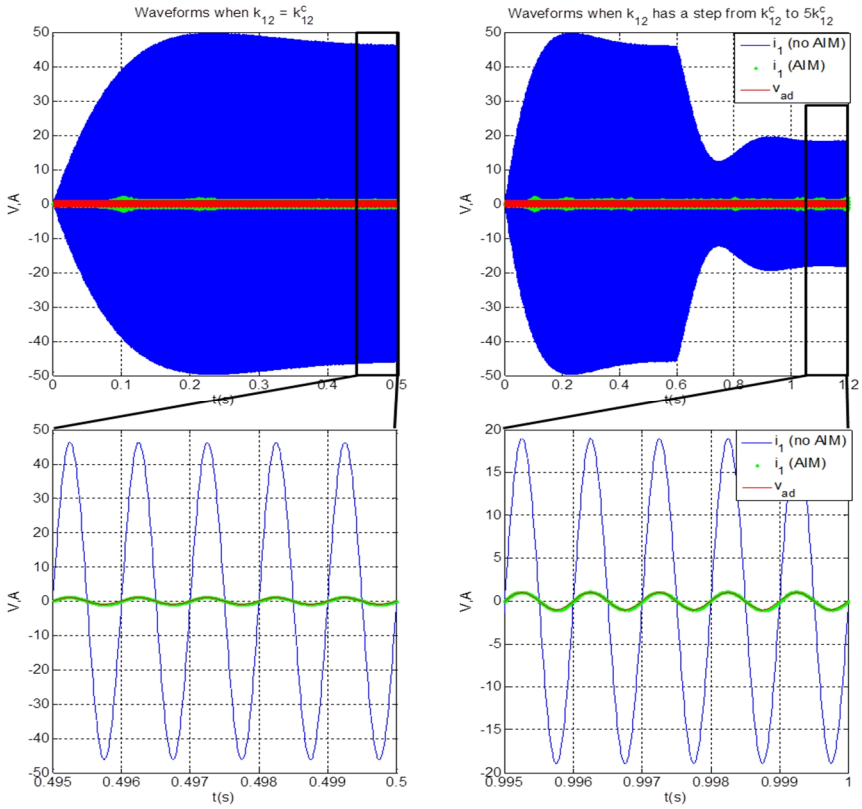


Figure 25 $v_{ad}$ , $i_1$ for simulation case 2, without and with AIM network for Simulink model

It can be seen that configuration with AIM network maintains current amplitude (and voltage source and transmitter current are still in phase), thus enabling optimal conditions for a higher power transfer.

### 5.3.3.3. Results for situation 3: switching frequency too close to operation frequency

Lowering switching frequency will not respect the required separation between boost converter dynamics (resonance, cut-off and switching frequencies); and, for very low values of $f_s$, Nyquist rate is not accomplished, so voltage source from which reference current is obtained will not be properly tracked. Besides, if switching frequency is located within antenna bandwidth, inductor current will have a ripple corresponding to $f_s$.

Figure 26 shows the allowed and prohibited values for $f_s$ in respect of operation frequency ( $f_{1,2} = f_{ad}$ ) and antenna bandwidth ($BW$). So as to evaluate deterioration in performance for low switching frequencies, $f_s$ is set to $f_{ad}$ ; inductor current for this dimension and the appropriate dimension ( $f_s = 100 f_{ad}$ ) are compared.

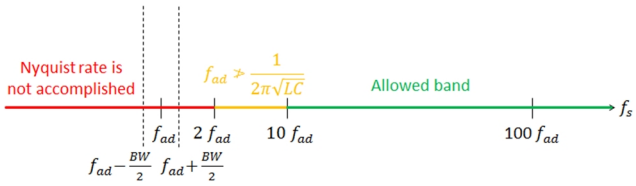


Figure 26 Frequency bands allowed or prohibited for $f_s$

As shown in Figure 27 (results from state-space equation model implemented with Simulink), waveforms obtained with lowered switching frequency do not longer correspond to the desired ones: inductor current is distorted and not matched in phase to voltage source, condition which is achieved for situation where separation between dynamics is maintained ( $f_s$ = $100 f_{ad}$).

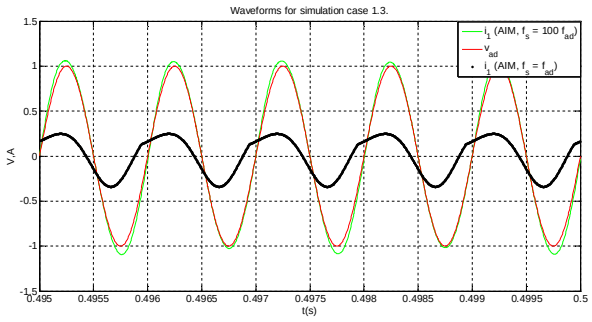


Figure 27 $v_{ad}$ , $i_1$ for simulation case 3 with state-space equation model

## 6. Conclusions and future development

New applications of RIC-WPT require exploration of new link configurations: asymmetrical systems and multi-point RIC-WPT networks. Furthermore, it is also necessary to analyse more demanding situations, such as a sudden change in operation conditions or several coupling scenarios.

Exploration includes prediction of link behaviour and optimal design before link deployment; and correction of performance and adaptation to operation conditions to enhance power transfer once the link is operative. Prior to exploration, a verification of existing models is required to check that analytical approach matches actual response when operating at these demanding scenarios.

Regarding identified challenges, in this work a critical comparison of existing antenna and link models is performed to guarantee analytical to actual behaviour correlation. Both frequency (FEKO, linear transfer functions approach, circuit-based PSPICE) and time domain models (state-space equations, circuit-based PSPICE) have been verified for several coupling scenarios.

Once analytical approach is verified, the RIC-WPT link is characterized in terms of link input impedance and resonant frequencies so as to predict its behaviour.

It is found that deviation from ideal operation conditions can be detected in link input impedance. On the one hand, its phase at operation frequency is different from zero if the link includes an interfering object (whose resonant frequency is not matched to that of transmitter and receiver), that is, resonant frequency of the link is shifted from its nominal value. This is detected as a phase mismatch between voltage source and transmitter current at operation frequency, and thus power factor in transmission, transmitted power and power at the load are lower.

On the other hand, resonant frequency of link input impedance is split to multiple resonances if coupling factor between transmitter and receiver is greater than its critical value, that is, if the link is operating at over-coupling regime. This is detected as a drop in transmitter current amplitude, and power transfer is lower.

Regarding expected deterioration in performance when the link operates out of nominal conditions, it is necessary to avoid that mismatch both before the link is deployed (by means of an optimal design) and once it is implemented (an adaptive energy management system is aimed to maintain optimal conditions when a change in operation conditions occurs).

To achieve the first point, a design methodology to optimize an asymmetric RIC-WPT link has been presented. It is observed that maximum achievable power transfer efficiency of frequency-optimized asymmetric links is more restrictive than that of frequency-optimized symmetric links, thus showcasing the impact of this study.

Concerning adaptive energy management, a PFC-based AIM network is proposed to enhance operation conditions once the link has been deployed. The proposed network can increment transmitted power, Power Factor in transmission and power at the load in a RIC-WPT link where transmitter and receiver are matched in resonance to operation frequency, and with an interfering object not matched in resonance to operation frequency. In addition to this, it provides robustness in front of a change in distance or alignment between transmitter and receiver (when there is no interfering element).

The proposed adaptive energy management system can achieve the desired robustness in front of a change in operation conditions and enhance power transfer for several coupling scenarios. However, analysis and simulation have only been performed for a SIMO link. Future steps in the line of this work deal with MIMO, RIC-WPT systems and link optimization taking into account transmitter and receiver front-ends simultaneously.

Analytical characterization of a MIMO, RIC-WPT link has already been studied [9], and a challenge is presented when the proposed concept of AIM network is expanded to the MIMO scenario: a change caused by the AIM network in a particular transmitter will affect link input and output impedances seen from the other nodes. Therefore, AIM networks will be necessary both in transmission and in reception, in order to enhance performance and provide robustness in front of interfering objects and interference caused by the rest of transmitters and receivers.

# Bibliography

[1] Assaf, M., Seshsachalam, D., Chandra, D., Tripathi R. K., "DC-DC Converters Via Matlab/Simulink", Electrical Engineering Department Motilal Nehru National Institute of Technology Allahabad, Utter Pradesh- 211004, India.

[2] C.A. Balanis, "Antenna Theory Analysis and Design", Wiley, 2005.

[3] Bou, E., Alarcon, E., Gutierrez, J., Sedwick, R., "Survey on Non-Radiative Resonant Inductive Coupling Wireless Power Transfer: A Critical Comparison of Alternative Theories", submitted to IEEE TCAS-I, 2012.

[4] Bou, E., El Aroudiy, A., Fisher, P., Alarcon, E., "Unveiling Nonlinear Dynamics in a Resonant Inductively Coupled Wireless Power Transfer Circuit", ISCAS 2014.

[5] Bou, E., Alarcon, E. and J. Gutierrez, "A comparison of analytical models for Resonant Inductive Coupling Wireless Power Transfer", *Progress in Electromagnetics Research Symposium*,2012.

[6] Bou, E., Alarcon, E., Sedwick, R., "Advances in Non-Radiative Resonant Inductive Coupling Wireless Power Transfer: a critical comparison of alternative circuit and system models driven by emergent applications", *Survey paper preamble for the Special Session "Circuital aspects of emergent application driven Wireless Power Transfer Systems"*, ISCAS, 2014.

[7] Bou, E., Alarcon, E., Sedwick, R., Fisher, P., "Interference analysis on Resonant Inductive Coupled Wireless Power Transfer links", *IEEE Transactions on Circuits and Systems*, May 19, 2013.

[8] Bou, E., Alarcon, E. and R. Sedwick, "Maximizing efficiency through impedance matching from a circuit-centric model of non-radiative resonant wireless power transfer," *Proceedings of 2013 IEEE International Symposium on Circuits and Systems*, June 2013.

[9] Bou, E., Sedwick, R., Alarcon, E., "Scalability Analysis of SIMO Non-Radiative Resonant Wireless Power Transfer Systems based on Circuit Models", submitted to IEEE International Symposium on Circuits and Systems. Melbourne, June 2014.

[10] Bou-Balust, E., Alarcón, E., "Wireless Power Transfer: Fueling the dots", Chiba University Auckland, June 6th 2014.

[11] Bryant, B., Kazimierczuk, M.K., "Open-Loop Power-Stage Transfer Functions Relevant to Current-Mode Control of Boost PWM Converter Operating in CCM", *IEEE Transactions On Circuits And Systems*—I: Regular Papers, Vol. 52, No. 10, October 2005.

[12] "Current Mode Hysteretic Buck Regulators", Application Report, Texas Instruments, 2013. [Online] Available: [http://www.ti.com/lit/an/snva170b/snva170b.pdf] [Accessed: January 2014].

[13] Erickson, Robert W., Maksimovik, Dragan, "Fundamentals of Power Electronics", 2nd ed. University of Colorado Boulder, USA: KLUWER ACADEMIC PUBLISHERS, 2001.

[14] "The Fourier Series of Selected Waveforms", [Online] Available: [http://people.clarkson.edu/~jsvoboda/Syllabi/EE221/Fourier/FourierSeriesTable.pdf] [Accessed: 8 January 2014].

[15] Grandi, G., Kazimierczuk, M. K., Massarini, A. and Reggiani U., "Stray Capacitances of Single-Layer Solenoid Air-Core Inductors", *IEEE Transactions On Industry Applications*, vol. 35, no. 5, September/October 1999.

[16] Garcia, Oscar, Cobos, Jose A., Prieto, Roberto, Alou, Pedro, Uceda, Javier, "Single Phase Power Factor Correction: A Survey", *IEEE Transactions on Power Electronics*, Vol.18, No.3, May 2003

[17] Hedlund, M., "Design and construction of a bidirectional DCDC converter for an EV application", Teknisk- naturvetenskaplig fakultet, Uppsala Universitet, Sweden, February 2010.

[18] Hee-Seung Kim, Do-Hyun Wono, Byung-Jun Jang, "Simple design method of wireless power transfer system using 13.56MHz loop antennas", Kookmin Power Electronic Center – KPEC, Department of Electrical Engineering, Kookmin university, Seoul, Korea, 2010.

[19] Kesler, Morris, "Highly Resonant Wireless Power Transfer: Safe, Efficient, and over Distance", WiTricity Corporation, 2013. [Online] Available:

[http://www.witricity.com/pdfs/highly-resonant-power-transfer-kesler-witricity-2013.pdf] [Accessed: 27 January 2014].

[20] Kiani, M. and Ghovanloo, M., "An RFID-Based Closed-Loop Wireless Power Transmission System for Biomedical Applications", *IEEE Transactions On Circuits And Systems—Ii: Express Briefs*, vol. 57, no. 4, April 2010.

[21] Kiani, M. and Ghovanloo, M., "The circuit theory behind coupled-mode magnetic resonance-based wireless power transmission," *Circuits and Systems I: Regular Papers*, *IEEE Transactions* on, no. 99, 2012.

[22] Kurs, A., Karalis, A. and Moffat, R., "Wireless power transfer via strongly coupled magnetic resonances," Science, vol. 6, pp. 83–86, June 2007.

[23] Lee, Y., "RFID Coil Design", Microchip Technology Inc., 2002. [Online] Available: [http://ww1.microchip.com/downloads/en/AppNotes/00678b.pdf] [Accessed: 8 January 2014].

[24] Liguang Xie, Yi Shi, Y. Thomas Hou, Wenjing Lou, "Wireless Power Transfer and Applications to Sensor Networks", Virginia Polytechnic Institute and State University, USA.

[25] Louganski, K. "Generalized Average-Current-Mode Control Of Single-Phase Ac-Dc Boost Converters With Power Factor Correction", *Dissertation for the degree of Doctor of Philosophy in Electrical Engineering*, Faculty of the Virginia Polytechnic Institute and State University, Blacksburg, Virginia, 2013.

[26] Perrott, M. H., "Comparison of Series and Parallel RC Circuits", OpenCourseWare , Massachusetts Institute of Technology, Cambridge, Massachusetts, 2003. [Online] Available: [http://ocw.mit.edu/courses/electrical-engineering-and-computer-science/6-976-high-speed-communication-circuits-and-systems-spring-2003/lecture-notes/lec3.pdf] [Accessed: 24 March 2014].

[27] "Power Factor Correction (PFC) Handbook. Choosing the Right Power Factor Controller Solution. HBD853/D", On-Semiconductor, Rev. 4, February 2011. [Online] Available: [http://www.onsemi.com/pub_link/Collateral/HBD853-D.PDF] [Accessed: 31 January 2014].

[28] Sample, Alanson P., Meyer, D. A., Scott T. Wisdom, Smith, J. R., "Analysis, Experimental Results, and Range Adaptation of Magnetically Coupled Resonators for Wireless Power Transfer", *IEEE Transactions On Industrial Electronics*, Vol. 58, No. 2, February 2011.

[29] Sample, Alanson P., Waters, B. H., Wisdom, S. T., Smith, J. R., "Enabling Seamless Wireless Power Delivery in Dynamic Environments", *Proceedings of the IEEE*, June 2013.

[30] Sedwick, R., "A fully analytic treatment of resonant inductive coupling in the far

field," *Annals of Physics*, 2012.

[31] Skanda, V., "Power Factor Correction in Power Conversion Applications Using the dsPIC® DSC", Microchip Technology Inc., 2007. [Online] Available: [http://ww1.microchip.com/downloads/en/appnotes/01106a.pdf] [Accessed: January 2014].

[32] "Towards practical deployability of Resonant Inductive Coupling: A Design Space Exploration of Distance and Frequency Effects." IEEE, January 2012.

[33] Zaohong Yang, "Recent Developments in High Power Factor Switch-mode Converters", IEEE Conference Publications, Department of Electrical and Computer Engineering, Queen's University, Kingston, Ontario, 1998.

[34] Zierhofer, C.M., Hochmair, E.S., "Geometric Approach for Coupling Enhancement of Magnetically Coupled Coils", *IEEE Transactions On Biomedical Engineering*, Vol. 43, No. 7, July 1996.

[35] Zolfagharifard, E., "Formation flying satellites", the Engineer, UK, May 2014. [Online] Available: [http://www.theengineer.co.uk/in-depth/formation-flying-satellites/1008738.article]. [Accessed: 17 May 2014].